AN EXPERIMENTAL INVESTIGATION OF SPHERICAL CAP BUBBLES IN LIQUIDS
SUNDELL, ROBERT ELMER
ProQuest Dissertations and Theses; 1971; ProQuest Dissertations & Theses Global

INFORMATION TO USERS

This dissertation was produced from a microfilm copy of the original document. While the most advanced technological means to photograph and reproduce this document have been used, the quality is heavily dependent upon the quality of the original submitted.

The following explanation of techniques is provided to help you understand markings or patterns which may appear on this reproduction.

1. The sign or "target" for pages apparently lacking from the document photographed is "Missing Page(s)". If it was possible to obtain the missing page(s) or section, they are spliced into the film along with adjacent pages. This may have necessitated cutting thru an image and duplicating adjacent pages to insure you complete continuity.

2. When an image on the film is obliterated with a large round black mark, it is an indication that the photographer suspected that the copy may have moved during exposure and thus cause a blurred image. You will find a good image of the page in the adjacent frame.

3. When a map, drawing or chart, etc., was part of the material being photographed the photographer followed a definite method in "sectioning" the material. It is customary to begin photoing at the upper left hand corner of a large sheet and to continue photoing from left to right in equal sections with a small overlap. If necessary, sectioning is continued again — beginning below the first row and continuing on until complete.

4. The majority of users indicate that the textual content is of greatest value, however, a somewhat higher quality reproduction could be made from "photographs" if essential to the understanding of the dissertation. Silver prints of "photographs" may be ordered at additional charge by writing the Order Department, giving the catalog number, title, author and specific pages you wish reproduced.

University Microfilms

300 North Zeeb Road
Ann Arbor, Michigan 48106

A Xerox Education Company

Reproduced with permission of the copyright owner. Further reproduction prohibited without permission.

72-17,184

SUNDELL, Robert Elmer, 1938-
AN EXPERIMENTAL INVESTIGATION OF SPHERICAL CAP BUBBLES IN LIQUIDS.

Yale University, Ph.D., 1971
Engineering, mechanical

University Microfilms, A XEROX Company, Ann Arbor, Michigan

© 1972

Robert Elmer Sundell

ALL RIGHTS RESERVED

THIS DISSERTATION HAS BEEN MICROFILMED EXACTLY AS RECEIVED.

Reproduced with permission of the copyright owner. Further reproduction prohibited without permission.

AN EXPERIMENTAL INVESTIGATION
OF
SPHERICAL CAP BUBBLES IN LIQUIDS

Robert E. Sundell

1971

A Dissertation

Presented to the Faculty of the Graduate School

of Yale University

in Candidacy for the Degree of

Doctor of Philosophy

Reproduced with permission of the copyright owner. Further reproduction prohibited without permission.

PLEASE NOTE:

Some pages may have

indistinct print.

Filmed as received.

University Microfilms, A Xerox Education Company

Reproduced with permission of the copyright owner. Further reproduction prohibited without permission.

Abstract

An experimental investigation of spherical cap bubbles in water and mineral oil was conducted. Steady rise-speeds of spherical cap bubbles in water were measured in 30 and 150 cm diameter tanks. The Reynolds number range of previous experiments was extended from 1×10^5 to 1.5×10^5. The geometry of spherical cap bubbles in water was investigated with shadowgraph photographs. It was found that the shapes of spherical cap bubbles in water are geometrically similar for variable bubble volumes. In addition, the structure of laminar and turbulent wakes was clarified and discussed in conjunction with new schlieren photographs. Also, wooden models of spherical cap bubbles were tested in water to investigate the effect of geometry on bubble motion.

The steady rise-speeds of spherical cap bubbles in mineral oil were measured in a 30 cm diameter tank. The results are in qualitative agreement with a theory by Parlange (1969). Finally, the bubble rise-speed corresponding to the onset of trailing gas "skirts" in high viscosity liquids was measured and compared to a recent theory of Parlange (1971).

Reproduced with permission of the copyright owner. Further reproduction prohibited without permission.

Acknowledgments

I wish to thank my thesis advisor, Professor Peter P. Wegener, for suggesting this research topic and for his continual interest and enthusiastic support. Special thanks go also to Professor Jean - Yves Parlange, whose theoretical work in this field was an important stimulus in the project. In addition, I wish to thank the other members of my thesis committee, Professors Daniel E. Rosner and Robert G. Wheeler, for their guidance and interest.

Financial support was provided by the Connecticut Research Commission under Contract RSA 70-8.

The aid of other members of the laboratory was invaluable, both in their assistance in photographic work and in their availability for discussions concerning experimental problems. These include Dominic Cagliostro, Benjamin Wu, Elihu Zimet, and Leo Smith. Also, Randy Morris gave important assistance in data reduction and graphics.

Finally, I especially wish to thank my wife, Gwyneth, for typing this thesis and providing the majority of the financial support during my years of graduate study.

Reproduced with permission of the copyright owner. Further reproduction prohibited without permission.

Contents

	page
Abstract.	i
Acknowledgments.	ii
Contents.	iii
I. Introduction.	1
II. Review of Bubble Motion in Liquids.	8
A. Motion of Spherical Drops and Bubbles.	8
B. Motion of Ellipsoidal Drops and Bubbles.	12
C. Motion of Spherical Cap Bubbles.	14
III. Spherical Cap Bubbles in Water.	23
A. Experimental Results and Procedures.	23
1. Rise-speed Results.	23
2. Measurements of Bubble Geometry.	26
3. Schlieren Photographs.	28
4. Drag Coefficient of Lenticular Wooden Models.	28
B. Summary of Results in Water.	32
IV. Spherical Cap Bubbles in Mineral Oil.	34
V. References.	37
Appendix 1: Description of Tank Laboratory.	40
Appendix 2: List of Symbols and Dimensionless Groups.	44
Appendix 3: List of Figure Captions.	46
Figures	49

Reproduced with permission of the copyright owner. Further reproduction prohibited without permission.

I. Introduction.

Knowledge of the mechanism of bubble motion is important in the many areas of engineering dealing with processes that involve the movement of gaseous "bodies" through liquids. Such processes include distillation, fermentation, fluidization, flotation, decarbonization in steel production, and many others (see, e.g., Brodkey, 1967). In addition, the possible application of bubble technology to solve such environmental problems as the eutrophication of lakes indicates the broad possibilities of work in this area.

The equation governing the motion of a bubble or drop is as follows:

$$\text{Drag} + \text{Buoyancy} = (\text{Mass} + \text{Virtual Mass}) \times \text{Acceleration}, \quad (1)$$

where one allows positive or negative net buoyancy forces. The virtual mass arises from the fact that when the velocity of the body changes, the total kinetic energy of the fluid must change also. It is found, however, that bubbles reach a constant terminal speed after traveling, at most, the distance of a few bubble diameters. We may then set the right hand side of eq. (1) equal to zero and we have for steady flow the balance of drag forces and buoyancy forces. This may be written as

Reproduced with permission of the copyright owner. Further reproduction prohibited without permission.

$$D - V\rho g + V\rho' g = 0 , \tag{2}$$

where ρ is the surrounding fluid (liquid) density, ρ' is the density of the bubble material, V is the bubble volume, and D is the drag force on the bubble.

In general, the drag on a bubble is a complicated function of its geometry, its speed, and the physical properties of the bubble material and medium. In turn, the bubble geometry depends on the hydrodynamic, the viscous, and the interfacial forces it experiences.

As a first step one can define the usual drag coefficient, c_D, by the equation

$$D = c_D \rho/2 \, U^2 A , \tag{3}$$

where A is the area of a representative bubble cross-section. Using eqs. (2) and (3) we may express the steady rise-speed, U, of a bubble by the following expression:

$$U^2 = \frac{2Vg}{\rho c_D A}(\rho - \rho') . \tag{4}$$

For gas bubbles $\rho' \ll \rho$; so we have

$$U^2 = \frac{2Vg}{c_D A} . \tag{5}$$

Reproduced with permission of the copyright owner. Further reproduction prohibited without permission.

The drag coefficient for a spherical bubble is found from eq. (5) to be

$$C_D = \frac{8}{3} g \frac{r}{U^2} \quad , \tag{6}$$

where r is the bubble radius. This expression allows one to determine the drag coefficient experimentally by measuring the size and steady rise-speed of a bubble. For non-spherical bubbles it is common to define an equivalent radius (see, e.g., Haberman and Morton, 1956) by the relation

$$\bar{r} = \left[V / \frac{4}{3}\pi \right]^{1/3} \quad , \tag{7}$$

and this length parameter is often used in eq. (6) in place of the spherical bubble radius, r.

If one considers only pure liquids (i.e., liquids free of surfactants with the surface tension, σ = constant along the bubble-liquid interface), the motion of a single bubble in an infinitely extended Newtonian liquid is described by the following eight variables: U, ℓ (characteristic bubble dimension), ρ, ρ', g, σ, μ (dynamic viscosity of the liquid medium), and μ' (dynamic viscosity of the bubble gas). Neglecting the density and viscosity of the bubble gas, relative to that of the liquid ($\rho'/\rho = 0(10^{-3})$ and $\mu'/\mu = 0(10^{-2})$ for air-water) leaves six variables and with the three dimensions of mechanics we expect three

Reproduced with permission of the copyright owner. Further reproduction prohibited without permission.

independent dimensionless parameters to govern the steady motion of bubbles in pure liquids. In addition to the drag coefficient, c_D, defined earlier, one may form such dimensionless groups as the Reynolds number,

$$R_e = \frac{2\ell U \rho}{\mu} , \tag{8}$$

the Weber number,

$$We = \frac{2\ell U^2 \rho}{\sigma} , \tag{9}$$

and a "liquid property" parameter,

$$M = \tfrac{3}{4} \frac{We^3}{Re^4} C_D = \frac{g\mu^4}{\rho\sigma^3} \tag{10}$$

Other dimensionless groups can be formed, but as is illustrated in eq. (10) only three will be independent. In particular, the Weber number gives the ratio of the hydrodynamic pressure forces to the surface tension forces on the bubble. The parameter, M, depends primarily on the dynamic viscosity of the liquid medium. The reason for this is the large range of viscosities which exists for liquids (e.g., $\mu \approx 10^3$ for castor oil, $\mu \approx 1$ cp for water) in contrast to the range of values of air-liquid surface tension ($\approx$20 to 75 $\frac{\text{dynes}}{\text{cm}}$) for common liquids. M takes on values of 10^{-2} to 10^{-7} for more viscous liquids such as mineral oil and

Reproduced with permission of the copyright owner. Further reproduction prohibited without permission.

glycerine ("slow" fluids) and it shows values of 10^{-8} to 10^{-10} for less viscous liquids as water and alcohol ("fast" fluids). The dimensional analysis then gives, for example,

$$f\ (c_D,\ Re,\ We) = 0, \tag{11}$$

$$f\ (c_D,\ Re,\ M) = 0, \tag{12}$$

and

$$f\ (c_D,\ We,\ M) = 0. \tag{13}$$

A bubble can assume various shapes when moving through a liquid (Haberman and Morton 1956). In particular, for pure water the bubble shape remains spherical for $We \lesssim 1$ corresponding to small bubbles ($r \lesssim 0.05$ cm) where the action of surface tension is dominant. For bubbles with radii greater than ~ 0.05 cm, variations of pressure over the bubble surface due to fluid motion tend to distort the bubble into an oblate ellipsoid moving perpendicular to its major axis. The bubble will then begin to wobble, oscillate or spiral. This corresponds to an apparent* drop in the bubble's rise-speed which normally increases with bubble size (Haberman and Morton 1956). For bubbles in "slow" fluids, such as mineral oil, the distortion from the spherical shape occurs, but the corresponding instability

---

* This may be due to the longer path (spiral or otherwise) followed by the bubble. This has not been accounted for by investigators (Haberman and Morton 1956; Hartunian and Sears 1957) when measuring bubble rise-speeds.

Reproduced with permission of the copyright owner. Further reproduction prohibited without permission.

and drop in rise-speed does not appear (Haberman and Morton 1956). For larger bubbles, where $V \geq 3$ cm^3 ($We \geq 20$) the bubble attains a characteristic "spherical-cap" shape. A steady rectilinear path is again followed. Spherical cap bubbles are shown in figures 2 and 3.

Using the three dimensionless groups given in eq. (12) and (13) respectively, Haberman and Morton (1956) correlated all bubble rise data available at the time and these are shown in figures 5 and 6 as taken from their paper. There is no completely systematic arrangement with changes in M evident from these curves. This could be due to scatter in the data used to draw the curves, or possibly the variables considered in the nondimensional parameters are insufficient for a complete description of bubble motion.* However, there seems to be a definite trend toward categorizing the bubbles in groups of M values. Particularly, figure 6 indicates a good correlation among the "fast" fluids ($M = 10^{-10}$ to 10^{-8}) and is clearly distinct from the "slow" fluids ($M = 10^{-7}$ to 10^{-2}). One also notes the constant drag coefficient for all liquids when $We \geq 20$, i.e., for spherical cap bubbles.

---

* The effect of surfactants, the effect of the tank walls, and the bubble-gas density and viscosity were neglected.

Reproduced with permission of the copyright owner. Further reproduction prohibited without permission.

The purpose of this work is to experimentally investigate many of the fluid mechanical phenomena associated with the rise of spherical cap bubbles in liquids. Before discussing the results of this investigation, a review of previous theoretical and experimental work on bubbles rising in liquids is presented.

Reproduced with permission of the copyright owner. Further reproduction prohibited without permission.

II. Review of Bubble Motion in Liquids.

A. Motion of Spherical Drops and Bubbles.

When the hydrodynamic pressure forces are weak relative to the surface tension forces on a bubble, the bubble shape tends to be spherical. In pure water this occurs for $We \lesssim 1$ and $r \lesssim .05$ cm. This corresponds to a Reynolds number in water as high as 200 so one expects boundary layer ideas to be useful for the "larger" spherical bubbles.

Considering first the regime where inertia forces are negligible, $Re << 1$, one recalls the well known solution for Stokes flow (1851) about a solid sphere which gives for the drag

$$D = 6\pi r \mu U . \tag{14}$$

With eqs. (6) and (8) this results in

$$c_D = \frac{24}{Re} , \tag{15}$$

From experiments on solid spheres it is found that actually eq. (15) holds quite well for $Re \lesssim 0.5$ (e.g., figure 4.9.2 on p. 234, Batchelor 1967). A second approximation to the solution of the complete equations for a solid sphere gives

$$c_D = \frac{24}{Re}(1 + \frac{3}{16} Re), \tag{16}$$

Reproduced with permission of the copyright owner. Further reproduction prohibited without permission.

This expression gives good results for Re $\lesssim$ 1 (p. 234 Batchelor 1967).

For spherical drops or bubbles the "no slip" boundary condition for solid bodies is replaced by the condition of continuous velocity components and continuous tangential stress across the interface. Again with Re $\ll$ 1 we have the solution of Hadamard (1911) and Rybczinski (1911) for flow about a "fluid sphere" which gives for the drag force

$$D = 6\pi r\mu U \frac{2\mu + 3\mu'}{3\mu + 3\mu'} \quad . \tag{17}$$

Once again for gas bubbles where $\mu' \ll \mu$ we have

$$D = 4\pi r\mu U \quad , \tag{18}$$

and using eqs. (6) and (8) we find

$$c_D = \frac{16}{Re} \quad . \tag{19}$$

The "fluid sphere" boundary conditions imply "pure fluids with σ = constant along the interface. Comparing eqs. (14) and (18) we see that

$$D_{solid} = (3/2)D_{fluid} \quad , \tag{20}$$

i.e., as intuitively apparent, the drag of a solid sphere is larger than that of a fluid sphere at a given Reynolds number.

Reproduced with permission of the copyright owner. Further reproduction prohibited without permission.

The drag coefficient for spherical bubbles as measured in three different "slow" fluids is shown in figure 4 as taken from Haberman and Morton (1956). It is noted that the experimental curves lie between the two limiting curves for $Re \ll 1$ discussed above. Also the experimental curves show that for decreasing Reynolds numbers the drag coefficient becomes equal to that of a rigid sphere. The boundary conditions for a "fluid" sphere seem to be invalid in this regime and the reason for this is not completely clear (see, e.g., Harper, Moore, and Pearson 1967).*

For higher Reynolds numbers (say $Re \approx 10^2$) where the bubble is still spherical, one expects that boundary layer concepts may be applied to obtain the solution for the drag. It can be shown that the jump in velocity across this boundary layer at a "free surface" is small [≈ 0 (boundary layer thickness)] (p. 366 Batchelor 1967) and this implies that:

(1) the tendency for back-flow to occur in the boundary layer in areas of negative pressure gradient is less than that for a rigid wall. Therefore, flow separation is likely to occur at higher Reynolds numbers for

---

* Surfactants present at the bubble-liquid interface would act to retard the terminal rise-speed of a spherical bubble with respect to that given by the "fluid-sphere" relation of eq. (18).

Reproduced with permission of the copyright owner. Further reproduction prohibited without permission.

spherical gas bubbles than for solid spheres. For a solid sphere, flow separation indicated by the formation of a small region of closed streamlines at the rear stagnation point occurs at Re $\approx$ 20 (p. 150, Van Dyke 1964 and Fig. 4.12.8, Batchelor 1967);

(2) since velocity gradients in the boundary layer are not of larger order than gradients outside the boundary layer, the dissipation of energy is of the same order throughout the fluid. The drag can then be calculated by determining the dissipation in the more extensive region of irrotational flow outside the boundary layer. This was first done by Levich (1949) and gives

$$c_D = \frac{48}{Re} \quad , \tag{21}$$

a result also obtained by Ackeret (1952). It may be noted that the drag coefficient for a rigid body from which the boundary layer does not separate is proportional to $Re^{-1/2}$ (p. 337, Batchelor 1967). Moore (1963) improved the estimate of the drag given by eq. (21) by calculating the dissipation in the boundary layer and wake to give

$$c_D = \frac{48}{Re}\left(1 - \frac{2.2}{Re^{1/2}}\right) \quad . \tag{22}$$

Figures 1 and 2 in Moore's paper indicate that eqs. (21) and (22) agree well with experiments in the limited range of Reynolds numbers where they apply (for spherical bubbles with

Reproduced with permission of the copyright owner. Further reproduction prohibited without permission.

$Re >> 1$), with eq. (22) showing better agreement than eq. (21). Eq. (21) is shown in figure 5.

B. Motion of Ellipsoidal Drops and Bubbles.

As noted earlier very small bubbles rise in rectilinear paths but in "fast" fluids ($M = 10^{-8}$ to 10^{-10}) with relatively small viscosity a critical size is reached at which the bubble suddenly assumes an oscillatory trajectory. This path may be helical or the bubble may oscillate in a given plane as it rises. The bubbles at this point are seen to be slightly deformed and have the shape of oblate ellipsoids. They move with their longer axis at right angles to the flow direction. For the case of more viscous liquids ($M = 10^{-2}$ to 10^{-7}) bubbles simply become more and more deformed as the size increases with no oscillations in shape or path.

Work has been done to study the conditions that exist when spherical bubbles begin to deform. Moore (1965) has shown for gas bubbles in steady flow in "low-M" fluids that the minimum and subsequent rise in c_D with Re (see figure 5) can be explained in terms of a transition from a spherical to an ellipsoidal shape. Taylor and Acrivos (1964) show by a perturbation technique for small Reynolds and Weber numbers ($Re \leq 1$, $We \leq 1$) that small bubbles will deform into oblate ellipsoids and finally approach a shape somewhat similar to that of a spherical cap bubble with

Reproduced with permission of the copyright owner. Further reproduction prohibited without permission.

further increases in the Weber number.

The stability of bubbles has been studied by Saffman (1956) and by Hartunian and Sears (1957). Hartunian and Sears experimentally determined the critical bubble size and terminal velocity in various "pure" liquids (free of surface-active substances) at the onset of instability. The critical bubble size was taken to be that at which the bubble would just begin to oscillate. From this, critical Reynolds and Weber numbers were calculated and the results are shown in figure 7 along with an average curve drawn through the data. Here Weber number is defined as $\widetilde{We} = U\sqrt{\frac{\rho r}{\sigma}}$ The results seem to indicate two distinct criteria for the onset of instability in rising gas bubbles. A branch of the curve is independent of the Weber number with a value of $Re \approx 200$ and the other branch for $Re > 200$ is independent of the Reynolds number with $\widetilde{We} \approx 1.26$. The stability curve is not analogous to the familiar stability diagrams in which a curve separates regions of stability from regions of instability. The actual meaning is that for any liquid capable of producing unstable bubbles, the critical Weber number and Reynolds number must be such as to fit somewhere on this curve. In addition, Hartunian and Sears also carried out an analysis that assumed the form of a general perturbation in the shape of a deformable sphere translating uniformly in an inviscid, incompressible fluid. The calculations lead to divergent solutions above a critical Weber

Reproduced with permission of the copyright owner. Further reproduction prohibited without permission.

number of $\widetilde{We}$ = 1.23 which is seen to be in excellent agreement with their experimental value for Re > 200. From figure 6 one also notes that for "low-M" liquids the minimum drag occurs at a fairly universal value of the Weber number. This value We ≈ 2 corresponds to $\widetilde{We} \approx 1$ which is in good agreement with the experimentally determined critical Weber number in figure 7.

C. Motion of Spherical Cap Bubbles.

When bubbles become so large that surface tension no longer plays a significant role, they attain a characteristic spherical cap shape (figure 3). This occurs in water for $V \gtrsim 2 - 3$ cm^3 and $We \gtrsim 20$ and the drag coefficient approaches a constant value of approximately 2.6 as seen in figure 5. The corresponding Reynolds numbers above which c_D = constant depend on the properties of the liquid and typical values are $Re \gtrsim 5{,}000$ for water and $Re \gtrsim 80$ for mineral oil (Haberman and Morton 1956).

As is evident from this range of Reynolds numbers, one expects different flow situations to arise. For the large Reynolds numbers that occur for spherical cap bubbles in water ($Re \approx 10^5$) one expects a large turbulent wake as illustrated in figure 1(b) (Davies and Taylor 1950). Here the bubble has a nearly perfect spherical top surface with a ragged underside. For lower Reynolds numbers ($Re \approx 10^2$) a laminar wake with closed streamlines is expected (Slaughter

Reproduced with permission of the copyright owner. Further reproduction prohibited without permission.

and Wraith 1968). This wake is illustrated in figure 1(a). Here the bubble has a spherical top surface with a smooth, slightly concave bottom.*

Davies and Taylor (1950) were first to advance a fluid mechanical model to determine the rise-speed of spherical cap bubbles without regard to the nature of the wake. They considered the steady flow near the stagnation point on the front face of the bubble and, with axes fixed relative to the bubble, applied Bernoulli's theorem for a streamline at the bubble surface. Neglecting the small pressure variation inside the bubble,** they assumed a constant pressure over the forward face giving

$$1/2\ u^2 = gh = g(R - r\cos\theta) \quad . \tag{23}$$

---

* Much confusion has existed concerning the wake behind spherical cap bubbles. From photographs taken by Davies and Taylor (1950), showing a spherical cap bubble followed by an almost spherical region of turbulent fluid with no motion behind, it has been conjectured that around the spherical region of turbulence the flow is potential flow which closes up smoothly behind, forming no wake. That this interpretation is incorrect is obvious from momentum arguments, and Maxworthy (1967) experimentally showed the existence of a wake.

** If the pressure is constant inside the bubble, it is constant outside as well, and neglecting "friction drag" we come to the surprising conclusion that there are no forces acting on it. However, we can see the reason for this if we write Newton's Second Law for the bubble

$$F = mg$$

and remember that we assumed the bubble to have zero mass.

Reproduced with permission of the copyright owner. Further reproduction prohibited without permission.

Here R is the radius of curvature of the bubble surface at the stagnation point, u is the local fluid velocity at the bubble surface, h is the positive vertical distance from the stagnation point and r, θ are spherical polar coordinates with origin at the center of curvature of the bubble surface (see figure 1(b)). Following Batchelor (1967) we assume u varies linearly with distance from the stagnation point (p. 105, Batchelor 1967). We may then write

$$u = \alpha U \theta \quad , \tag{24}$$

where α is a dimensionless constant dependent only on the bubble shape and U is the steady terminal bubble speed as before. Since R is the radius of curvature at the stagnation point, we have for the front bubble surface

$$r = R + O(\theta^3) \quad , \tag{25}$$

with the terms of order θ and θ^2 being zero because of the definition of R. Expanding the right-hand side of eq. (23) for small θ and with eq. (24) and eq. (25) we have

$$\alpha^2 U^2 = gR \quad . \tag{26}$$

This expression relates the steady speed of rise of a bubble with the local radius of curvature of the bubble surface at the stagnation point and depends on a particular

Reproduced with permission of the copyright owner. Further reproduction prohibited without permission.

bubble shape only through the constant factor α.* Davies and Taylor noted that the front bubble surface was essentially spherical and that the boundary layer that detached at the bubble edge seemed to lie roughly on the same sphere as the front bubble face (figure 1, Davies and Taylor 1950). Therefore, they assumed the velocity distribution over the front face of the bubble to be that of irrotational flow about a sphere of radius R, which gives (from, e.g., Batchelor 1967)

$$u = 3/2\ U \sin\theta \quad . \tag{27}$$

From eq. (24) we have $\alpha = 3/2$ and using eq. (26) we find, finally,

$$U = 2/3\ (gR)^{1/2} \quad . \tag{28}$$

It is interesting to note that this relation has been found to agree well with experiments both in the high-M liquids where one expects a closed laminar wake (Davenport et. al. 1967) and in low-M liquids where a turbulent wake is expected (Davies and Taylor 1950).

Collins (1966) sought a second approximation to the Davies and Taylor expression by a perturbation of the

---

* For example with this relation Grace and Harrison (1967) calculated the rise-speeds of elliptical cap bubbles which occur when a large bubble encloses a surface (e.g., a rod) as it rises.

Reproduced with permission of the copyright owner. Further reproduction prohibited without permission.

spherical form. This gave a 2% correction to the constant in eq. (28) and resulted in a bubble shape indistinguishable from spherical over a large region near the front stagnation point. Also, Rippin and Davidson (1967) assumed a free streamline model for large gas bubbles in liquids and their results predict a bubble shape very similar to that of large spherical cap bubbles in low-M liquids. However, rise-speeds predicted by their model are 20% higher than experimental values.

Parlange (1969) has given a solution for the case of spherical cap bubbles with closed laminar wakes in high-M liquids. This model predicts that for Re >> 1 (but small enough to still have a laminar wake) the flow consists of a Hill's spherical vortex (see p. 526, Batchelor 1967) with irrotational flow outside. The flow in any plane through the axis of symmetry is shown in figure 1(a) with a circular closed streamline separating the region of vorticity from the irrotational flow outside. The theory gives for the steady rise-speed

$$U = \tfrac{1}{3}\left(\frac{4}{10\pi}\right)^{1/3} g^{2/3}\left(\rho/\mu\right)^{1/3} V^{1/3} \quad , \tag{29}$$

where here we note the rise-speed can be calculated from a known bubble volume unlike eq. (28) that requires knowledge of the bubble geometry. A second approximation to eq. (29) assuming a boundary layer outside the closed circular

Reproduced with permission of the copyright owner. Further reproduction prohibited without permission.

streamline gives for the steady bubble rise-speed

$$U = U_o \left[1 + (6.6 - 0.14 \ln Re_o)(9 Re_o)^{-1/2} \right] \qquad (30)$$

where U_o is the speed given by eq. (29) and $Re_o = 2R\rho U_o/\mu$.

Theoretical estimates of the half angle, Θ_{max}, (see figure 1(b)) for spherical cap bubbles have been given by Moore (1959), Rippin and Davidson (1967) and Collins (1967). These estimates were for low-M liquids and ranged from 39° to 60° depending on the chosen model. Davies and Taylor (1950) measured values of Θ_{max} for spherical cap bubbles in nitrobenzene (low-M liquid) and found values that scattered between 36° and 64° with a mean value of approximately 52° . There was no evident trend of Θ_{max} with bubble volume at the higher volumes.

It has been found experimentally, however, that in high-M liquids Θ_{max} increases as the Reynolds number decreases (Grace 1970). This has also been predicted by Parlange (1969) who gives an expression good for small Θ_{max} for bubbles in high-M liquids as follows

$$\Theta_{max} \simeq (4/3\ 80)^{1/4} Re^{-1/4} , \qquad (31)$$

where again Re is calculated using the bubble frontal radius, R.

For a given bubble geometry one recalls eq. (11)

Reproduced with permission of the copyright owner. Further reproduction prohibited without permission.

which gives a relationship between the three dimensionless parameters c_D, Re, and We. It has been noted that for spherical cap bubbles surface tension effects are negligible and eq. (11) reduces to

$$f\ (c_D, \mathrm{Re}) = 0 \quad . \tag{32}$$

Also, if one assumes fully turbulent wakes for spherical cap bubbles in low-M liquids, it is expected that viscosity effects can be neglected (i.e., neglecting the small friction drag). This gives finally

$$f\ (c_D) = 0 \quad , \tag{33}$$

or equivalently

$$c_D = \text{constant} \quad , \tag{34}$$

and the result implies that only inertial forces are important in the flow field. The result also implies that spherical cap bubbles with different volumes are geometrically similar (i.e., Θ_{max} = constant).

It was noted for bubbles in high-M liquids, such as mineral oil, that Θ_{max} increases with decreasing Re and one expects the drag coefficient, c_D, to depend on the Reynolds number. This also follows from the model for spherical cap bubbles with laminar wakes given by Parlange (1969) where

Reproduced with permission of the copyright owner. Further reproduction prohibited without permission.

$$C_D = 6\left\{20 R_e^{-1}\left[1 + (0.14 \ln R_e - 6.6) R_e^{-1/2}\right]\right\}^{1/3} . \qquad (35)$$

Finally, it has been observed that "skirts" or thin envelopes of air sometimes trail spherical cap bubbles in high-M liquids, such as mineral oil or glycerin (Davenport et. al. 1967, Angelino 1966, also figure 2). These skirts were also observed by Guthrie and Bradshaw (1969) who estimated their thickness to be about 40 microns by collecting the air contained in the skirt and measuring its volume. Parlange (1971) has also predicted the critical bubble rise-speed necessary for the onset of trailing gas skirts by balancing the hydrodynamic and surface tension forces at the edge of the spherical cap bubble and gives

$$U_{crit} = \frac{\sigma}{3\mu} \frac{\pi - \theta_{max} + \sin\theta_{max}\cos\theta_{max}}{\sin^2\theta_{max}\, tg(\theta_{max}/2)} . \qquad (36)$$

The purpose of this work is to further investigate many of the interesting and unique fluid mechanical phenomena associated with the rise of spherical cap bubbles in both low-M liquids (e.g., water) and high-M liquids (e.g., mineral oil). In particular, spherical cap bubbles are studied in water to determine if the drag coefficient is constant over a large range of bubble volumes as is suggested by dimensional analysis. Along with this the bubble angle, θ_{max}, is measured to note if any change in geometry occurs for large bubble volumes. Collin's (1965) experiment in

Reproduced with permission of the copyright owner. Further reproduction prohibited without permission.

a "two-dimensional" tank showed the wake of a cylindrical cap bubble in water to consist of a large stable vortex-pair for Reynolds numbers of the order 10^4. He predicts a wake consisting of a toroidal vortex (i.e., a Hill's spherical vortex) for three-dimensional spherical cap bubbles in water. However, Crabtree and Bridgewater (1967), also using a two-dimensional tank filled with water, showed vortex shedding to occur at a comparable Reynolds number. Therefore, the wake of spherical cap bubbles in water is here investigated to determine if Collin's conjecture is true or if vortex shedding occurs for three-dimensional bubbles at the higher Reynolds numbers (i.e., $Re \approx 10^4$ to 10^5).

Finally, the steady rise-speeds of spherical cap bubbles in mineral oil (a high-M liquid) are measured and compared with the prediction of Parlange (1969) (i.e., eqs. (29) and (30)). In addition, the theoretical prediction for the onset of the trailing gas "skirts" (i.e., eq. (36) Parlange 1971) is tested by experiments in mineral oil.

Reproduced with permission of the copyright owner. Further reproduction prohibited without permission.

III. Spherical Cap Bubbles in Water.

A. Experimental Results and Procedures.

1. Rise-speed Results.

Spherical cap bubbles in filtered* tap water were studied in a 150 cm diameter tank (see Appendix 1). Preliminary results were also obtained in a 30 cm diameter plastic tank. The bubbles were formed by tilting a plugged inverted funnel which had been filled with air. Some practice was required to produce large bubbles free of trailing "satellite" bubbles. The bubble volumes were measured by catching the bubble in an inverted funnel - graduated cylinder arrangement mounted at the top of the tank. The perfect gas law was used to correct this measurement to obtain the volume at the stations where the rise-speed was measured.** Light stations consisting of photo cells and parallel light beams produced by a He-Ne gas laser were used with an electronic counter to measure the steady bubble rise-speeds. The position of the light stations on the tank was varied to ascertain that the rise-speed was

---

* A 5-micron Cuno "Micro-Klean" water filter was used.

** The bubble volume changes less than 2% across the interval used to time the rise-speed.

Reproduced with permission of the copyright owner. Further reproduction prohibited without permission.

indeed steady.* Also, by installing two 3 x 4 ft. rectangular inserts at various positions in the large tank to determine the onset of "wall effects" it was determined that perturbations of the steady bubble rise-speeds were negligible for the bubble volumes investigated. Finally, a sufficient time interval was allowed between successive tests to make certain that residual vorticity in the liquid caused by previous bubbles was negligible. This time interval was checked by observing a dye-streak in the water.

The steady rise-speed of spherical cap bubbles in filtered water vs. (bubble volume)$^{1/3}$ is shown in figure 8. The bubble volumes measure from 3 cm^3 to 350 cm^3. This graph includes results from the 150 cm tank and the 30 cm tank. The effect of the walls on the rise-speeds in the 30 cm tank are seen to occur at $V^{1/3} \approx 3.5$ cm. The walls cause an increase of liquid motion downward with respect to the bubble, resulting in a decrease of bubble speed

---

* It is found that bubbles attain a constant rise-speed after traveling a distance of only a few bubble diameters. Following Batchelor (1967, p. 452) this can be shown for the case of a spherical bubble in irrotational flow where he derives the virtual mass of the bubble to be $1/2\rho V$ where again ρ is the liquid density and V is the bubble volume. Neglecting the real mass of the bubble gives for the equation of motion

$$\dot{U} = 2g \qquad (37)$$

Solving this for a typical spherical bubble with r = .06 cm and a terminal velocity of 30 cm/sec gives ~ 0.24 cm, or two bubble diameters, as the distance traveled before attaining steady speed.

Reproduced with permission of the copyright owner. Further reproduction prohibited without permission.

relative to that in an infinite medium. The rise-speeds in mineral oil also shown will be discussed in a later section.

A dimensionless group often used in the study of bubble motion is the Froude number defined as

$$Fr = \frac{U}{(g\ell)^{1/2}} \quad . \tag{38}$$

This is seen to be the square root of the ratio of inertia forces to buoyancy forces in the flow field. It is formally "equivalent" to the drag coefficient defined earlier in eq. (6) since the two are related by the expression

$$c_D = (8/3)Fr^{-2} \tag{39}$$

The Froude number for the water results in the 150 cm tank is plotted vs. the Reynolds number in figure 9. Both Fr and Re are calculated using the equivalent radius $\bar{r}$ as the characteristic length, ℓ , in eqs. (8) and (38). It is noted that the Froude number (or equivalently, c_D) is essentially constant over the large range of bubble volumes tested and the experimental results show a mean value of $Fr \approx 1.02$. This corresponds to $c_D = 2.55$. These results are also compared in the figure with those calculated from other sources. For the lower Reynolds numbers at which their data is taken we note agreement although substantial scatter exists in the results of Davies and Taylor (1950).

Reproduced with permission of the copyright owner. Further reproduction prohibited without permission.

Their results are for spherical cap bubbles in nitrobenzene which has approximately the same viscosity as water (i.e., $\mu \approx 1.0$ cp for water, $\mu \approx 1.8$ cp for nitrobenzene). In addition to the nitrobenzene results, Davies and Taylor (1950) also report experiments in water. Their results show considerable scatter and are not shown in the figure. However, their proposed mean value is equivalent to $Fr \approx 1$, in good agreement with the result stated above. A point taken from the experimental curves of Haberman and Morton (1956) is also shown in the figure.

Using the mean value of the Froude number measured above, we find from eq. (38)

$$U = 1.02 \sqrt{g\bar{r}} \quad , \tag{40}$$

which gives the rise-speed in terms of $\bar{r}$ or equivalently $V^{1/3}$. This equation is shown in figure 10 where the bubble rise-speeds are plotted after eliminating measurements showing wall effects.

2. Measurements of Bubble Geometry.

The frontal radii, R, of the bubbles were measured by taking full scale shadowgraph pictures with an optical system described in Appendix 1. A series of circular templates were used to measure the frontal radius of each bubble. To the accuracy of the measuring technique (within about 5%) a constant radius was found over the entire front

Reproduced with permission of the copyright owner. Further reproduction prohibited without permission.

face of the bubble.* (Davis and Taylor (1950) also measured a constant radius for spherical cap bubbles in nitrobenzene.) The bubble rise-speeds shown in figures 8 and 10 are plotted vs. $R^{\frac{1}{2}}$ in figure 11. The expression derived by Davies and Taylor (eq. (28)) is included and the results lie slightly below the theory. However, a curve through the results gives a slope of approximately 0.65 in good agreement with the theory. Davies and Taylor's (1950) results for spherical cap bubbles in nitrobenzene showed a slope of 0.655.

It can be shown that for a spherical cap shape (assuming a flat bottom) V, R, and Θ_{max} (see figure 1(b)) are related by the following geometrical relation

$$\cos^3\Theta_{max} - 3\cos\Theta_{max} + 2 = {}^{3V}/_{\pi R^3} \qquad (41)$$

By measuring the bubble volume and frontal radius, the angle, Θ_{max}, can be calculated. Values for Θ_{max} are shown in figure 12 for a large range of bubble volumes. The results show some scatter but an average value of $\Theta_{max} \approx 46^\circ$ is noted at the higher volumes. This value was checked by measuring the angle, Θ_{max}, directly from several of the photographs and the same average value was found. Consistent with our findings of c_D = constant for spherical cap

---

* This is strictly true only for bubbles with $V \gtrsim 15$ cm^3. For smaller bubbles the top surface is generally not smooth (see figure 3).

Reproduced with permission of the copyright owner. Further reproduction prohibited without permission.

bubbles, no obvious trend of Θ_{max} with bubble volume is noted.

3. Schlieren Photographs.

Schlieren photographs* were taken of spherical cap bubbles in the large tank to determine the nature of the wake. Examples are shown in figure 3 for a range of bubble volumes and show clearly a turbulent wake. A sharp delineation of the edge of the turbulent motion is noted. In particular, it is interesting to note the vortex that seems to be shedding off the main wake in the lower portion of figure 3,B. Also, the wake of larger bubbles ($V \gtrsim 100$ cm^3) seems to contract a short distance behind the bubble as seen in figure 3,D. The Reynolds numbers calculated with the frontal bubble radii, R, range from 2×10^4 for the 7.5 cm^3 bubble to 9×10^4 for the 151 cm^3 bubble.

4. Drag Coefficient of Lenticular Wooden Models.

To further study the effect of bubble geometry on bubble motion, it was decided to build three wooden models

---

* Fluid motions in the wake cause pressure and temperature changes which affect the index of refraction of the water by creating density gradients. For the velocities associated with bubble motion it can be shown that variations in the refractive index are the result of slight temperature differences in the water (Bland and Pelick 1962). A well aligned schlieren system can detect temperature changes in water of 0.01 C° (Waxler and Weir 1963).

Reproduced with permission of the copyright owner. Further reproduction prohibited without permission.

of spherical cap shape (assuming a flat bottom). The frontal radius of the three models was kept the same (R = 2.54 cm) but the half-angle, θ_{max}, was varied and took on values of $\theta_{max} = 30^{\circ}$, 52° and 75° respectively. The models were released at the bottom of the tank and allowed to rise to the surface. Small weights attached to the models by threads (in the manner of a drogue) were used to stabilize the models to prevent rocking, etc. The steady rise-speeds were measured, and knowing the net buoyancy forces and dimensions of the models, we can determine from eqs. (2) and (3) the drag coefficient, c_D.* Here, A in eq. (3) was taken to be the area of the base of the model. The results of these tests are shown in figure 13 where c_D is plotted vs. θ_{max}. Also shown are the results of Davies and Taylor (1950) who determined the drag coefficient for models with an identical geometry with the exception that on one model $\theta_{max} = 55^{\circ}$ rather than our 52°. These values of c_D were calculated by integrating measured pressures on the models and they also took A to be the base area of the model. The Reynolds number of the water model tests ranged from 0.5×10^4 to 1.7×10^4 and the frontal radius of the model was used to calculate Re. The Reynolds number of the Davies and Taylor tests was not given. It is noted that both sets of data give the same trend of c_D with θ_{max} but differ slightly

---

* The drag of the small weights was neglected.

Reproduced with permission of the copyright owner. Further reproduction prohibited without permission.

as to absolute value. This is due partially to the fact that the Davies and Taylor measurements neglect skin friction. Also, the tests may have been conducted at different Reynolds numbers. The increase of c_D for decreasing Θ_{max} is consistent with expectation since one would guess that as the flow effectively separates further upstream on the model (it is forced to do so by cutting off the model closer to the stagnation point) the drag (being mostly "form" drag for high Re) would increase. As Θ_{max} decreases the model approaches the shape of a circular disk and this limiting drag coefficient is indicated on the figure. Also shown is the drag coefficient for a sphere (Batchelor, 1967). Both values of c_D were taken for Re $\approx 10^4$ where the boundary layer separating from the sphere is still laminar. It is noted that c_D for our tests at $\Theta_{max} = 30^\circ$ is approximately equal to that of a circular disk.

An interesting result follows if we take eqs. (2) and (3) and write for the balance of drag and buoyancy forces on a spherical cap bubble

$$c_D \rho/2 \, U^2 A = \rho g V \quad . \tag{42}$$

We will again assign A to be the base area and we have for the spherical cap shape

$$A = \pi R^2 \sin^2 \Theta_{max} \quad , \tag{43}$$

where R is the frontal radius. Substituting this into eq. (42)

Reproduced with permission of the copyright owner. Further reproduction prohibited without permission.

and grouping terms in a convenient manner gives

$$C_D = \frac{3}{2} \frac{4/9 qR}{U^2} \frac{3V}{\pi R^3} \frac{1}{\sin^2 \theta_{max}} \quad . \tag{44}$$

Recalling the Davies and Taylor result given by eq. (28) and the geometrical relation, eq. (41), gives for the drag coefficient of spherical cap bubbles

$$C_D = \frac{3}{2} \frac{\cos^3 \theta_{max} - 3\cos \theta_{max} + 2}{\sin^2 \theta_{max}} \quad . \tag{45}$$

This is shown in figure 13 and it is interesting to note that c_D increases with θ_{max}, a behavior opposite to that of rigid models with the same shape as spherical cap bubbles.* A similar trend of c_D with θ_{max} for bubbles with a laminar wake can be noted from eqs. (31) and (35) given earlier as derived by Parlange (1969). One may also derive the equivalent of eq. (45) using $A = \pi \bar{r}^2$ where $\bar{r}$ is the equivalent radius defined in eq. (7). This gives

$$C_D = 3.8 \left[\cos^3 \theta_{max} - 3\cos \theta_{max} + 2 \right]^{1/3} \tag{46}$$

The constant value $c_D = 2.55$ as found earlier was calculated

---

* From eq. (42) we note that since $U^2 \propto V^{1/3}$ (eq. (40)), A must increase as $V^{2/3}$ for c_D to remain approximately constant for increasing θ_{max}. Since the base area, A, increases more slowly than $V^{2/3}$ for increasing θ_{max}, the drag coefficient must increase.

Reproduced with permission of the copyright owner. Further reproduction prohibited without permission.

using $\bar{r}$ as the characteristic length. Therefore, we may check this value by substituting our average $\theta_{max} = 46^{\circ}$ into eq. (46). This gives $c_D \approx 2.40$, slightly below the measured value, $c_D = 2.55$. However, we note that the measured rise-speeds shown in figure 11 are slightly below those predicted by eq. (28) which was used to derive eq. (45) and (46). Taking account of this error gives excellent agreement with the measured value $c_D = 2.55$. We note, then, that we have self-consistent measurements of c_D (or Fr), θ_{max} and U.

B. Summary of Results in Water.

Measurements of the rise-speed of spherical cap bubbles in water were extended to larger bubble volumes and correspondingly larger Reynolds numbers (from 1×10^5 to 1.5×10^5) than were hitherto seen in the literature. Moreover, the experimental uncertainties were much reduced. It was found that θ_{max} = constant = 46° and, therefore, that the shapes of spherical cap bubbles in water are geometrically similar for different bubble volumes.* ** Accordingly, it was found that c_D = constant = 2.55 (or

---

* The half-angle, θ_{max}, was measured for bubbles with volumes ranging from 7 cm^3 to 350 cm^3.

** Grace (1970) gives results that show θ_{max} to increase for spherical cap bubbles with $Re_{\bar{r}} \lesssim 10^2$.

Reproduced with permission of the copyright owner. Further reproduction prohibited without permission.

alternatively Fr = constant = 1.02) as predicted by dimensional analysis. The values found for θ_{max} and c_D differ somewhat from previous investigators (e.g., Siemes (1954) gives $c_D = 2.8$, $\theta_{max} \approx 52^{\circ}$) but they are found to be self-consistent. Davies and Taylor (1950) give a mean value of Fr $\approx$ 1, a value remarkably close to that stated above considering the large amount of scatter in their results.

Schlieren photographs of the wakes show a clearly turbulent structure even for the smallest observed spherical cap bubble ($V \approx 2$ cm^3, $Re_{\bar{r}} \approx 4.5 \times 10^3$). Collin's prediction that the wake would consist of a stable toroidal vortex for Reynolds numbers of the order of 10^4 appears to be false. Vortex shedding was noted for smaller bubbles ($V \approx 15$ cm^3) in agreement with the findings of Crabtree and Bridgewater (1967). However, it is likely that some type of recirculation exists directly behind the bubble as required by continuity of the liquid. Also, 8 mm movies taken of the wake give evidence of circulation behind the bubble. Such circulation may be hidden inside the turbulent structure seen in the photographs of figure 3.

Reproduced with permission of the copyright owner. Further reproduction prohibited without permission.

IV. Spherical Cap Bubbles in Mineral Oil.

Figure 2 shows spherical cap bubbles in mineral oil rising in a 30 cm diameter tank. Their apparent shape is distorted owing to the fact that they were viewed through a cylindrical tank wall. In figures 2(b) to 2(d) we note the appearance of partial and complete trailing gas "skirts".

The viscosity of the mineral oil is very sensitive to temperature which was carefully monitored during the oil experiments to detect any change. The oil viscosity was measured with a Hoeppler viscometer. In addition, small steel spheres (0.8 mm diam.) were dropped into the oil. Their Reynolds number was about 10^{-1} and by measuring the fall velocity, the viscosity could be determined directly from Stoke's law (see eq. (14)). These results confirmed the measurements made with the Hoeppler viscometer.

Typically for mineral oil we have $Re \approx 10^{2}$ using again the frontal radius, R, as the characteristic bubble dimension. A laminar closed wake was observed behind the bubble by viewing directly the motion of small spherical bubble swarms introduced prior to a test.

In figure 8 we have plotted the rise-speed results as taken in the 30 cm tank. Bubbles were tested in oil at two different viscosities as noted in the figure. Again

Reproduced with permission of the copyright owner. Further reproduction prohibited without permission.

the effect of the walls is noted for $V^{1/3} \gtrsim 4$ cm. In figure 10 the measured rise-speeds are shown after eliminating measurements showing wall effects. The results for $\mu = 119$ cp seem to agree with the water results and eq. (40) whereas the rise-speeds in the colder and, therefore, more viscous oil ($\mu = 229$ cp) show a lower value. This finding possibly implies a larger Θ_{max} than that measured for the water bubbles and, therefore, a higher drag coefficient and lower rise-speed (see Grace 1970). The Reynolds numbers for the bubbles in water and oil are also indicated on the figure. It is surprising that the results are so close considering the difference in Reynolds numbers and corresponding wake structure.

In figure 14 the rise-speeds are compared with eqs. (29) and (30). For the Reynolds numbers where the theory of Parlange (1969) is applicable ($Re \approx 10^2$), the results are in qualitative agreement with the theory but lie slightly below the prediction of the higher order approximation.

Finally, in figure 15 results are shown on the incidence of the trailing gas "skirts" following spherical cap bubbles in viscous (high-M) liquids. The viscosity of the mineral oil was varied by changing its temperature. This was done by lowering the temperature in the room to insure constant equilibrium conditions. The corresponding

Reproduced with permission of the copyright owner. Further reproduction prohibited without permission.

change in surface tension was found to be negligible.* The bubble rise-speed was measured which corresponded to the onset of a trailing gas "skirt" (figure 2). This critical rise-speed, U_{crit}, is shown as a function of the dynamic viscosity of the oil. It is noted that higher viscosities give lower critical speeds. Parlange (1971) has developed a simple model for the critical rise-speed necessary to overcome interfacial tension between liquid and gas at the sharply rounded edge of the bubble. His prediction (eq. (36)) is shown in the figure. The proper trend is indicated but the results lie above the predicted curve.

---

* The surface tension of the mineral oil was measured with a Cenco No. 70530 tensiometer.

Reproduced with permission of the copyright owner. Further reproduction prohibited without permission.

References

Ackeret, J. 1952
Z. angew. Math. Phys. 3, 259.

Angelino, H. 1966
Chem. Eng. Sci. 21, 541.

Arnold, H. D. 1911
Phil. Mag. 22, 755.

Batchelor, G. K. 1967
An Introduction to Fluid Dynamics, Cambridge University Press.

Bland, R. E., and Pelick, T. J. 1962
J. Basic Eng., ASME Trans., Ser. D., 587

Bond, W. N., and Newton, D. A. 1928
Phil. Mag. & J. Sci. V, Seventh Series, 794.

Brodkey, Robert S. 1967
The Phenomena of Fluid Motions, Addison - Wesley.

Bryn, T. 1933
Forschung 4, 27.

Collins, R. 1965
Chem. Eng. Sci. 20, 851.

Collins, R. 1966
J. Fluid Mech. 25, 469.

Crabtree, J. R., and Bridgewater, J. 1967
Chem. Eng. Sci. 22, 1517.

Davenport, W. G., Richardson, F. D., and Bradshaw, A. V. 1967
Chem. Eng. Sci. 22, 1221.

Davies, R. M., and Taylor, G. I. 1950
Proc. Roy. Soc. Lond. 200, Ser. A., 375.

Garabedian, P. R. 1957
Proc. Roy. Soc. Lond. 241, Ser. A., 423.

Grace, J. R. 1970
J. Chem. Eng. 48, 30.

Reproduced with permission of the copyright owner. Further reproduction prohibited without permission.

Grace, J. R., and Harrison, D. 1967
Chem. Eng. Sci 22, 1337.

Guthrie, R. I. L., and Bradshaw 1969
Chem. Eng. Sci. 24, 913.

Haberman, W. L., and Morton, R. K. 1956
Trans. Am. Soc. Civ. Eng. 121, 227.

Hadamard, J. 1911
Comptes Rendus, Acad. Sci., Paris, 152, 1735.

Harper, J. F., and Moore, D. W. 1968
J. Fluid Mech. 32, 367.

Harper, J. F., Moore, D. W., and Pearson, J. R. A. 1967
J. Fluid Mech. 27, 361.

Hartunian, R. A., and Sears, W. R. 1957
J. Fluid Mech. 3, 27.

Hill, M. J. M. 1894
Phil. Trans. Roy. Soc. 185, 213.

Levich, V. G. 1949
Zh. Eksptl. i. Teoret. Fiz. 19, 18.

Maxworthy, T. 1967
J. Fluid Mech. 27, 367.

Moore, D. W. 1959.
J. Fluid Mech. 6, 113.

Moore, D. W. 1963
J. Fluid Mech. 16, 161.

Moore, D. W. 1965
J. Fluid Mech. 23, 749.

Parlange, J.-Y. 1969
J. Fluid Mech. 37, 257.

Parlange, J.-Y. in preparation (1971)

Rippin, D. W. T., and Davidson, J. F. 1967
Chem. Eng. Sci. 22, 217.

Rybczynski, W. 1911
Bull. Acad. de Sci. de Cracovie (Series A), 40.

Reproduced with permission of the copyright owner. Further reproduction prohibited without permission.

Saffman, P. G. 1956
J. Fluid Mech. 1, 249.

Shoemaker, P. D., and Marc De Chazal, L. E. 1969
Chem. Eng. Sci. 24, 795.

Siemes, W. 1954
Chem. Ing. Techn. 26, 614.

Slaughter, I., and Wraith, A. E. 1968
Chem. Eng. Sci. 23, 932.

Stokes, G. G. 1851
Trans. Cambridge Phil. Soc. 9, Part II, 8.

Taylor, T. D., and Acrivos, A. 1964
J. Fluid Mech. 18, 466.

Van Dyke, M. V. 1964
Perturbation Methods in Fluid Mechanics, Academic Press, New York.

Waxler, R. M., and Weir, C.E. 1963
J. Research NBS 67A, 163.

Reproduced with permission of the copyright owner. Further reproduction prohibited without permission.

Appendix 1

Description of the Tank Laboratory

A schematic drawing and photograph of the tank facility are shown in figures 16 and 17 respectively. The steel tank is five feet in diameter and five feet in height and is constructed in two sections. When bolted together the two sections have a capacity of 700 gallons. The tank is equipped with six 18-inch and two 3-inch diameter windows as shown in the figures. Two of the 18-inch windows are optically flat for use in accurate shadowgraph and schlieren photography. A laser was used to align these two windows parallel by reflecting the beam back into the laser from each window. The tank bottom is equipped with a 6-inch diameter port to provide access for air lines, pipes, etc.

Tanks are located in the basement under the facility for storage of test liquids. A Randolph pump (Model 610, 200 gallons per hour capacity) is used to transfer the liquid from the basement to the tank facility.

A 4-foot diameter base-plate is situated at the bottom of the tank. An array of 1/4 inch holes were drilled and tapped in the plate to facilitate the mounting of equipment in the tank. This plate can be raised from the tank by means of an overhead 1-ton electric hoist. The hoist is installed on a track which extends over the tank facility.

Reproduced with permission of the copyright owner. Further reproduction prohibited without permission.

This arrangement allows one to change a set-up on the base plate without draining the tank.

Spherical cap bubbles are produced by a mechanism mounted on the base plate. This consists of an inverted funnel (plugged to hold air) which can be turned upright to release a slug of air into the tank. Some practice is required to produce large bubbles in water free from trailing satellite bubbles.

Bubble volumes are measured by catching the bubble in an inverted funnel-graduated cylinder arrangement mounted at the top of the tank. Graduated cylinders having capacities of 25, 50, 100, and 200 c.c. are used depending on the bubble size and give volumes to $\pm$ 0.5, $\pm$ 0.5, $\pm$ 1, and $\pm$ 1 c.c. respectively. This volume is then corrected for the pressure at the depth where bubble rise-speeds are measured.

Instrumentation

Light stations to measure the steady rise-speed of bubbles are mounted on the tank as shown in figures 16 and 18. These consist of photoelectric cells and a He-Ne continuous gas laser (University Laboratories Model 240, 1.0 mW) used with beam splitters. The photoelectric cells and beam splitters travel on vertically-mounted light benches to allow continuous positioning of the light stations

Reproduced with permission of the copyright owner. Further reproduction prohibited without permission.

along the tank. The laser and beam splitters provide two collimated beams that cross the tank. When a bubble interrupts a beam, a photocell activates a Simpson digital electronic counter (Model 2724) which measures the time interval between light paths to the nearest millisecond. The position and separation of the two beams can be varied to ascertain that the rise-speed is steady.

The beams are aligned by using three plumb lines, one at each of two windows and one at the center of the tank along the bubble path. The distance over which the bubble is to be timed is marked on the plumb lines and the laser beams can be accurately aligned with these points. The bubbles were timed over an interval of 8 $\pm$ 1/32 inches at the top window of the tank.

A schematic drawing of the shadowgraph-schlieren system is shown in figure 19. This system employs two 9 1/2-inch diameter parabolic first-surface mirrors of 79-inch focal length. The light source consists of a PEK 107 high pressure mercury-arc lamp with a DC power supply. A lens focuses the light source onto a 1 mm. wide slit. The slit is located at the focal point of one of the first-surface parabolic mirrors. It was necessary to bend the beam 90° because of space limitations. The resulting parallel beam is directed through the tank to the other parabolic first-surface mirror. This mirror focuses the parallel

Reproduced with permission of the copyright owner. Further reproduction prohibited without permission.

beam giving an image of the rectangular source at the mirror's focal point. Here part of the light is intercepted by a vertical knife edge. The image of the center of the tank is then focused on the ground-glass screen of a camera back. The optical path lengths are adjusted to give approximately 1:1 magnification of bubble and wake. A sphere of known diameter was positioned at the center of the tank and photographed to determine the exact magnification.

Photographs are taken by placing a shutter behind the 1 mm. slit as shown in the figure. A 1/1000 second exposure is sufficient to give a sharp picture of the bubble and wake. The light intensity is varied by use of neutral-density filters. Polaroid High Contrast, Type 51, 4x5 film and Kodak Plus-X Pan Professional 5x7 sheet film were used.

Reproduced with permission of the copyright owner. Further reproduction prohibited without permission.

Appendix 2

List of Symbols and Dimensionless Groups

A	cross sectional area
c_D	drag coefficient, eq. (3) and (6)
D	drag force
F	force
Fr	Froude number, eq. (38)
g	acceleration of gravity
h	coordinate
ℓ	characteristic bubble dimension
m	mass
M	liquid property parameter, eq. (10)
r	radius, polar coordinate
$\bar{r}$	equivalent radius, eq. (7)
R	radius of curvature at bubble stagnation point
Re	Reynolds number, eq. (8)
u	local flow speed
U	steady rise-velocity of bubble
V	bubble volume
We	Weber number, eq. (9)
α	dimensionless constant
ρ	density of liquid medium
ρ'	density of bubble material
σ	surface tension
μ	dynamic viscosity of liquid medium
μ'	dynamic viscosity of bubble material

Reproduced with permission of the copyright owner. Further reproduction prohibited without permission.

θ angle, polar coordinate

θ_{max} bubble half-angle

Reproduced with permission of the copyright owner. Further reproduction prohibited without permission.

Appendix 3

List of Figure Captions

1 Schematic sketch of a laminar (a) and turbulent (b) spherical cap bubble and nomenclature.

2 Photographs of spherical cap bubbles with and without "skirts" rising in mineral oil in a 30 cm tank. $\mu \approx 100$ to 200 cp, $V \approx 50$ to 100 cm^3.

3 Schlieren photographs of spherical cap bubbles rising in water in a 150 cm tank, $\mu = 1$ cp.

4 Drag coefficient of spherical bubbles as a function of Reynolds number. Experiments and theories in the low Reynolds number range.

5 Drag coefficient of bubbles of varying shape at higher Reynolds numbers.

6 Experiments on drag coefficients as a function of Weber number.

7 Stability envelope for the rectilinear motion of small spherical bubbles rising in pure liquids after Hartunian and Sears (1957) and experimental results on the onset of instability.

8 Measured rise-speed of all experiments with spherical cap bubbles.

Reproduced with permission of the copyright owner. Further reproduction prohibited without permission.

9 Froude number as a function of Reynolds number based on equivalent sphere radius from Yale data in a 150 cm tank and from other laboratories. $Fr \simeq 1.02$ as used in equation (40).

10 Rise-speed of spherical cap bubbles in water and mineral oil and prediction of equation (40). Reynolds number scales based on radius of curvature of the cap.

11 Rise-speed of spherical cap bubbles in water as a function of the frontal bubble radius. Comparison with equation (28).

12 Measured half-angle of spherical cap bubbles in water.

13 Drag coefficients of lenticular models tested in water and in a wind tunnel. Comparison with equation (45) for spherical cap bubbles.

14 Rise-speed of spherical cap bubbles in mineral oil at $\mu = 229$ cp in a 30 cm tank. Comparison with the Parlange (1969) theory for closed laminar wakes.

15 Critical rise speed for "skirt" formation of spherical cap bubbles in mineral oil in a 30 cm tank as a function of dynamic viscosity. Comparison with the theory of equation (36).

16 Drawing of the Yale 150 cm tank.

Reproduced with permission of the copyright owner. Further reproduction prohibited without permission.

17 Photograph of the Yale 150 cm tank.

18 Photograph of one of the viewing windows with timing light beams and multiple exposures showing a spherical cap bubble rising in water.

19 Schematic drawing of the optical system of the Yale tank.

Reproduced with permission of the copyright owner. Further reproduction prohibited without permission.

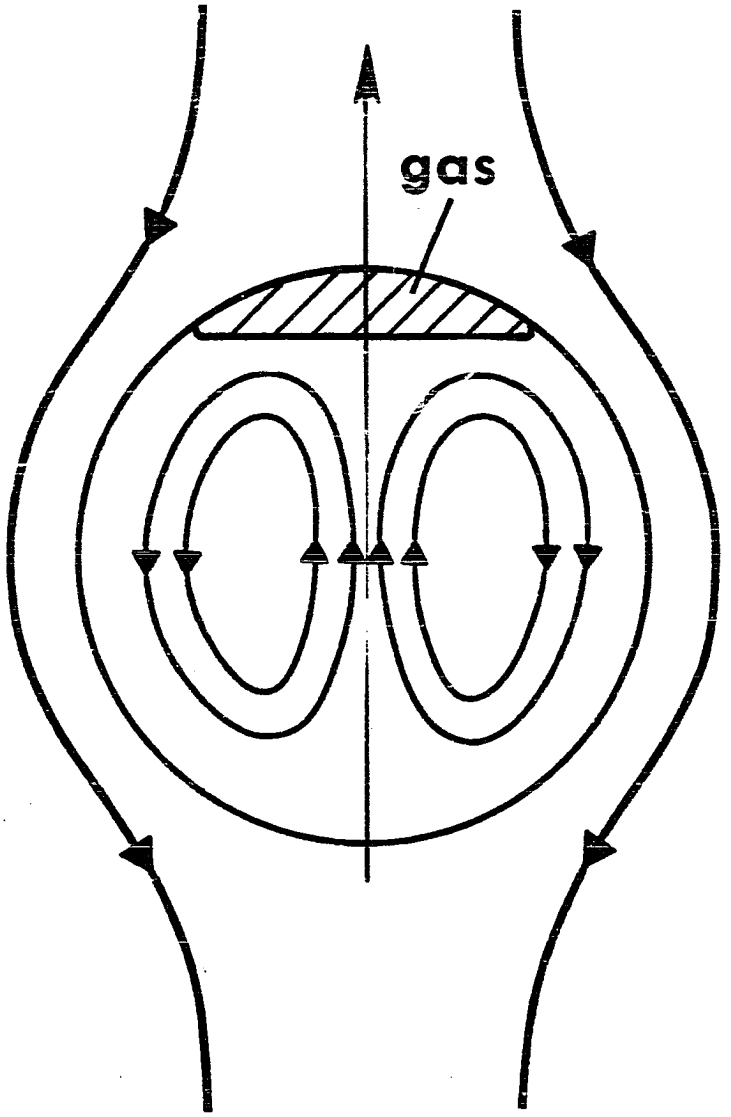

(a)

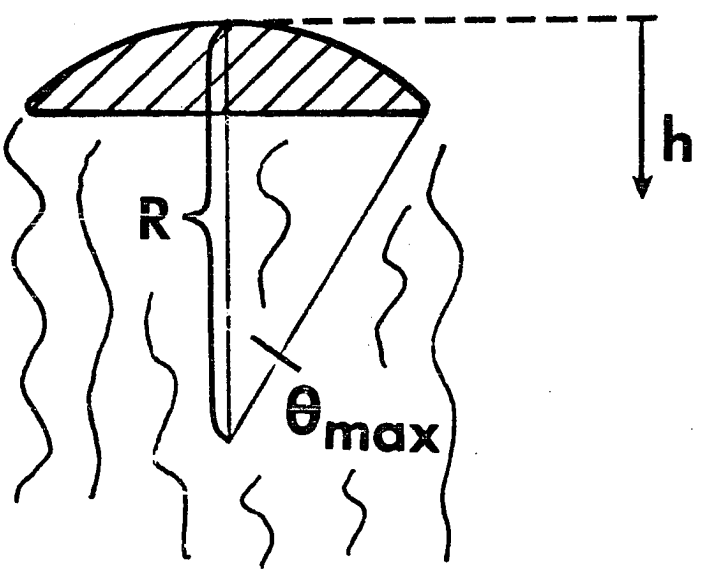

(b)

Reproduced with permission of the copyright owner. Further reproduction prohibited without permission.

Fig. 2

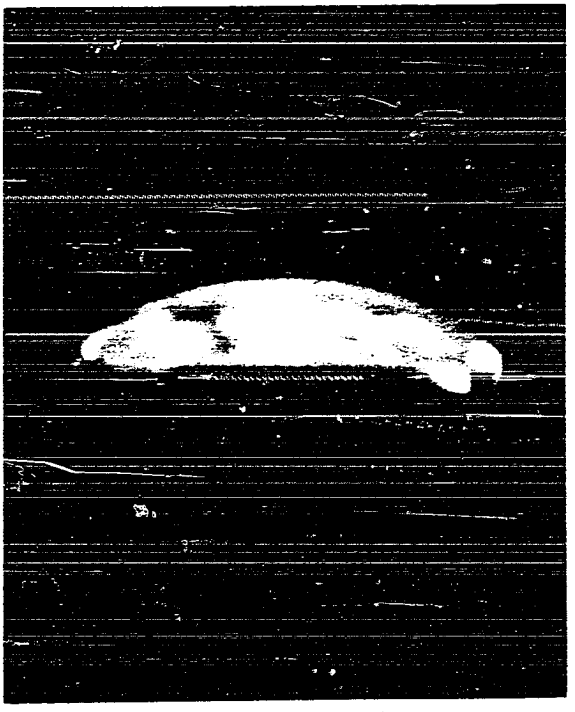

A

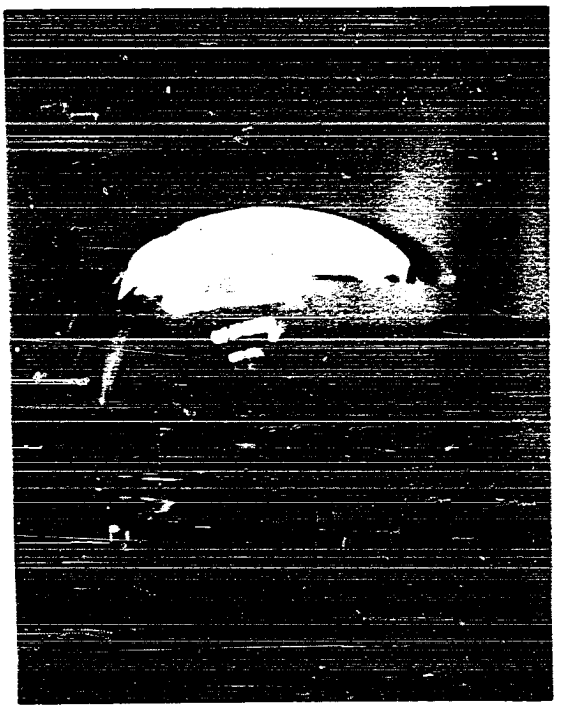

B

C

D

Reproduced with permission of the copyright owner. Further reproduction prohibited without permission.

Fig. 4

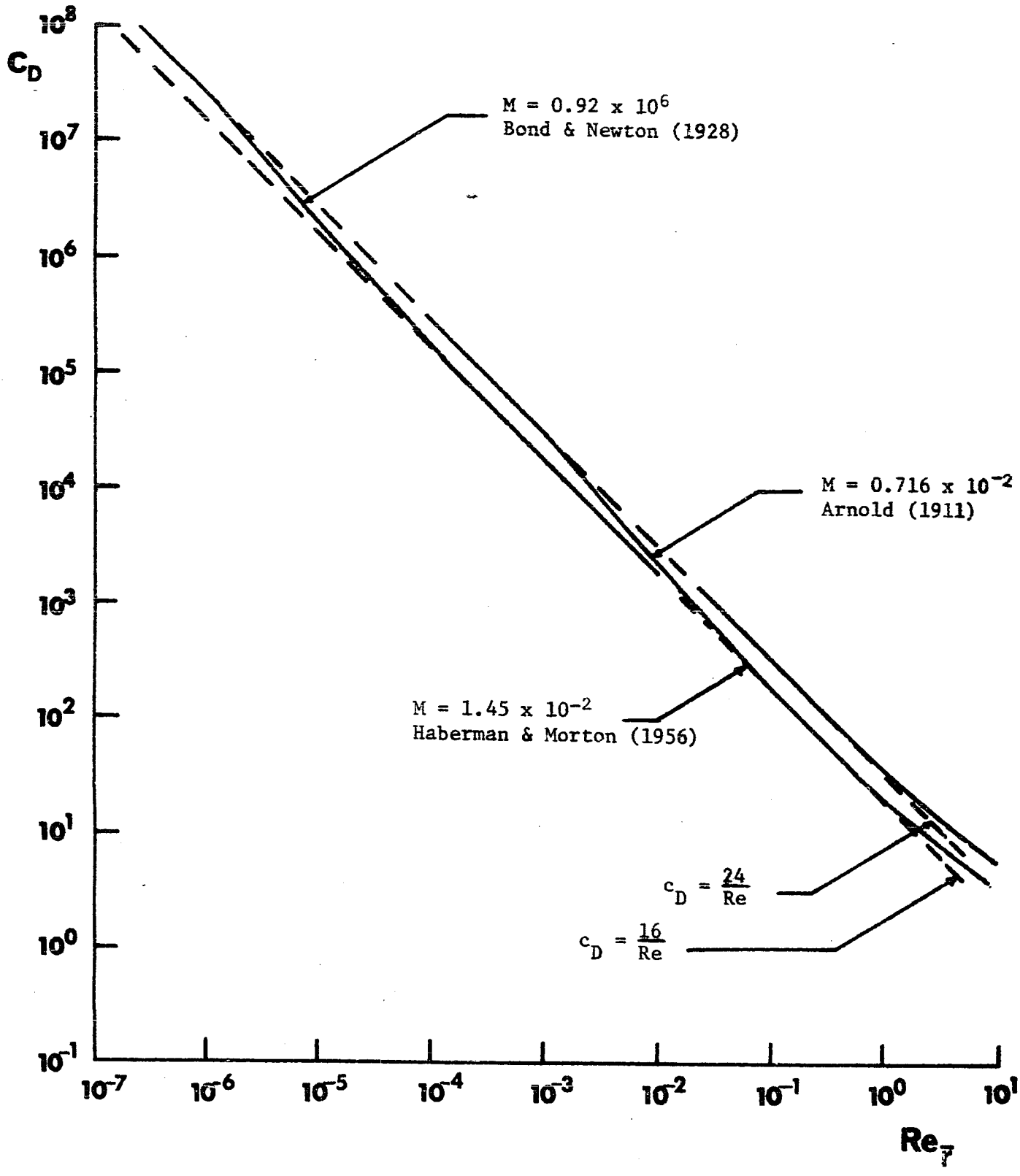

Reproduced with permission of the copyright owner. Further reproduction prohibited without permission.

Fig. 5

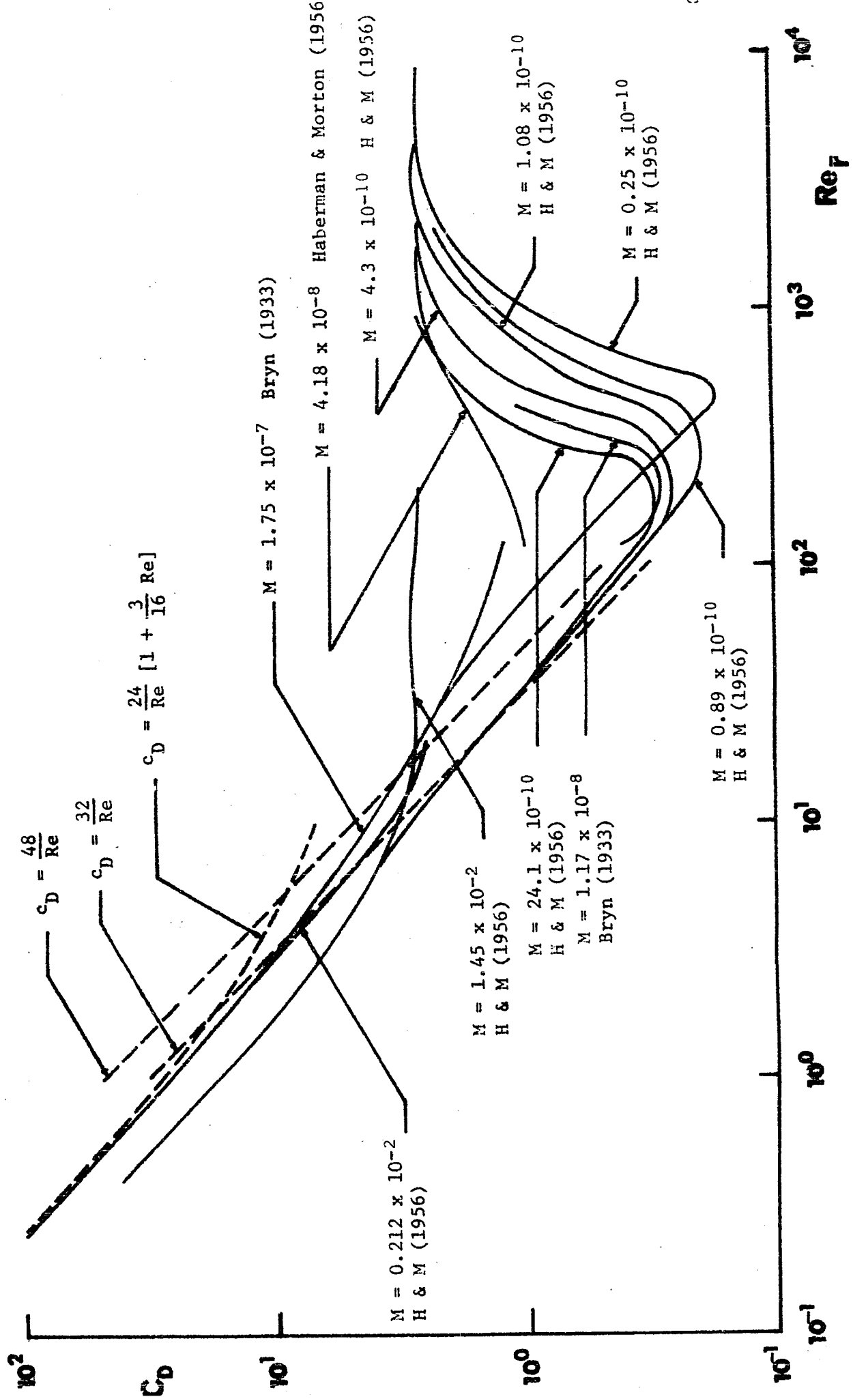

Reproduced with permission of the copyright owner. Further reproduction prohibited without permission.

Fig. 6

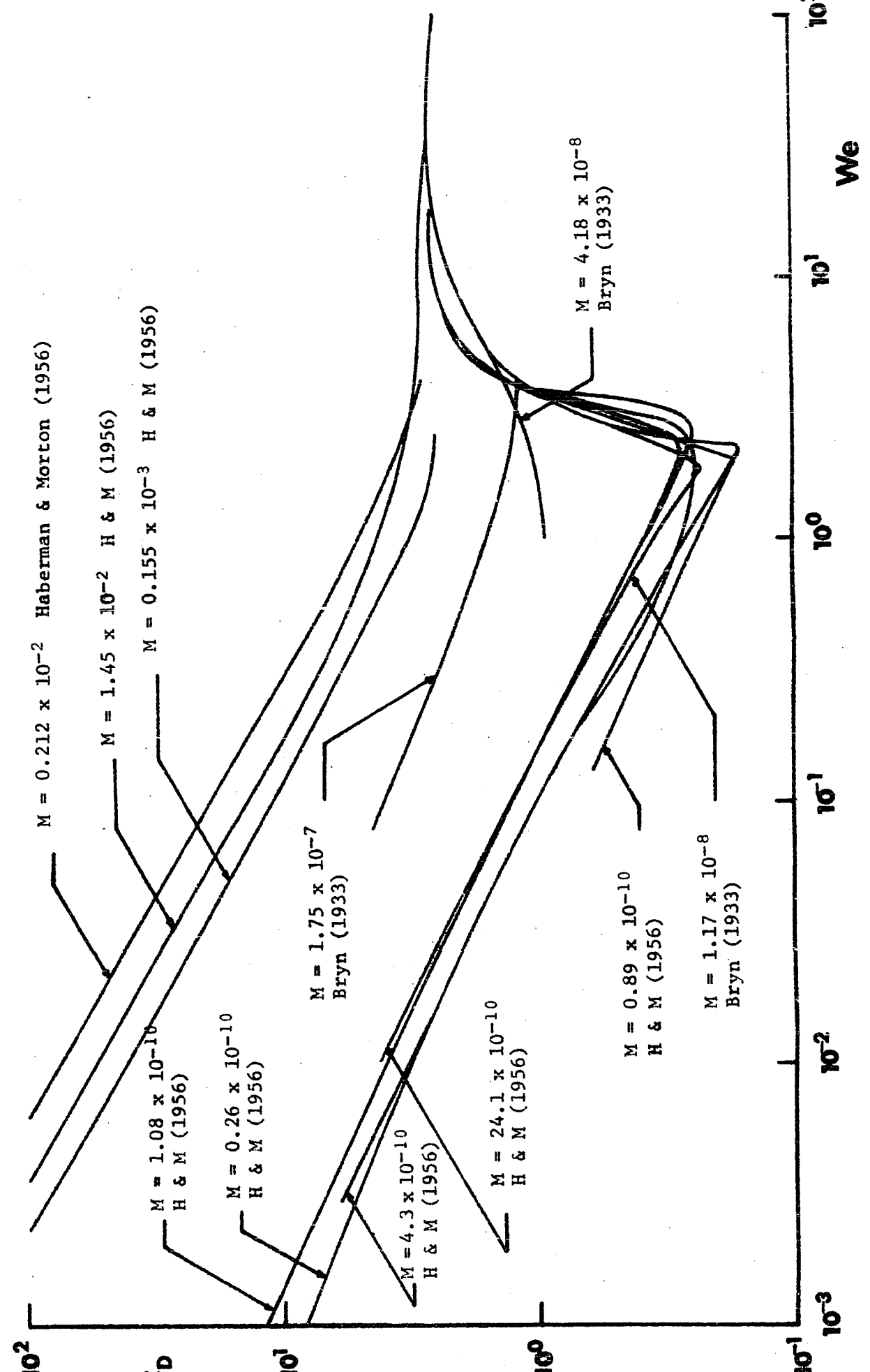

Reproduced with permission of the copyright owner. Further reproduction prohibited without permission.

Fig. 7

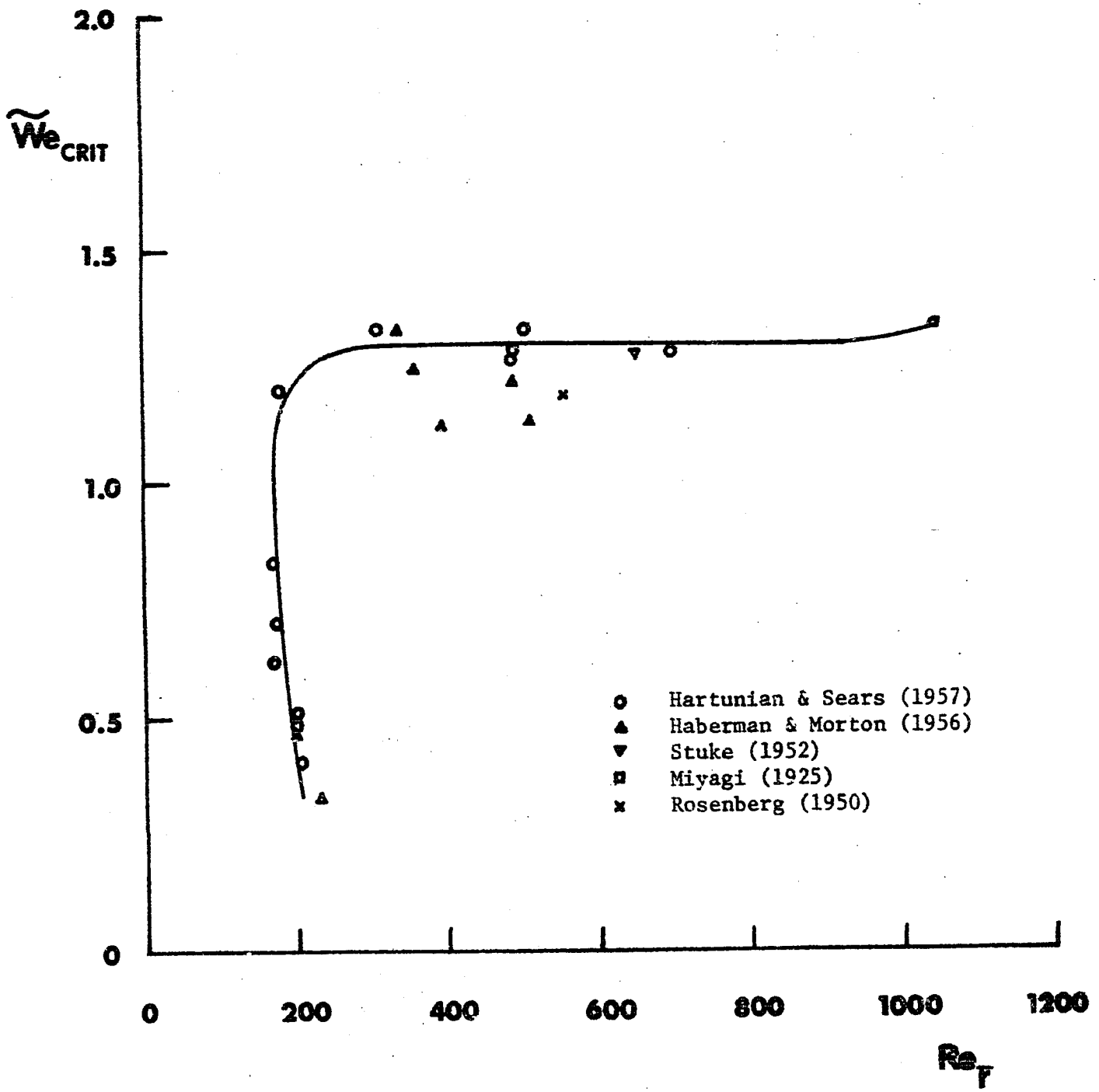

Reproduced with permission of the copyright owner. Further reproduction prohibited without permission.

Fig. 8

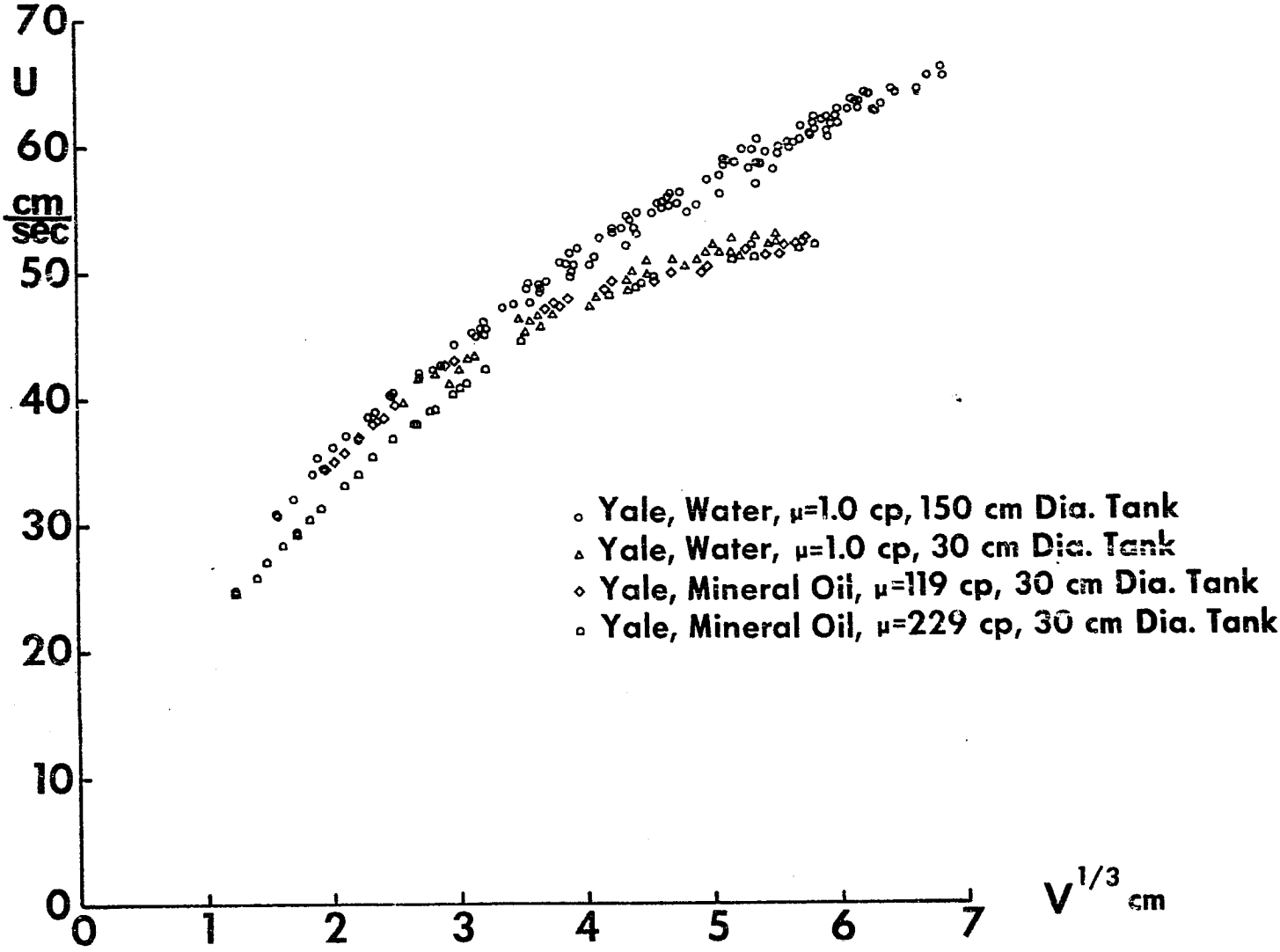

Reproduced with permission of the copyright owner. Further reproduction prohibited without permission.

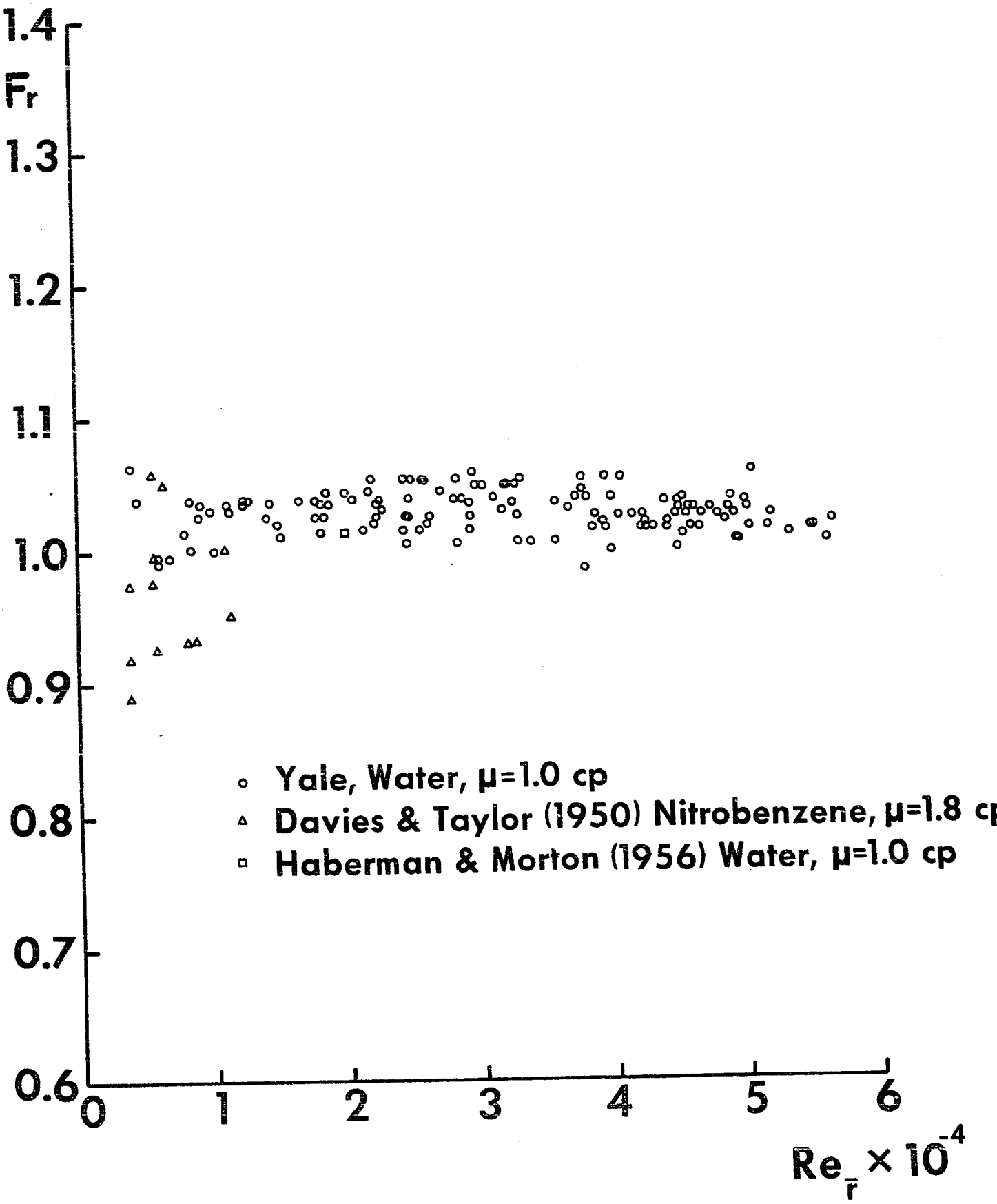

Reproduced with permission of the copyright owner. Further reproduction prohibited without permission.

Fig. 10

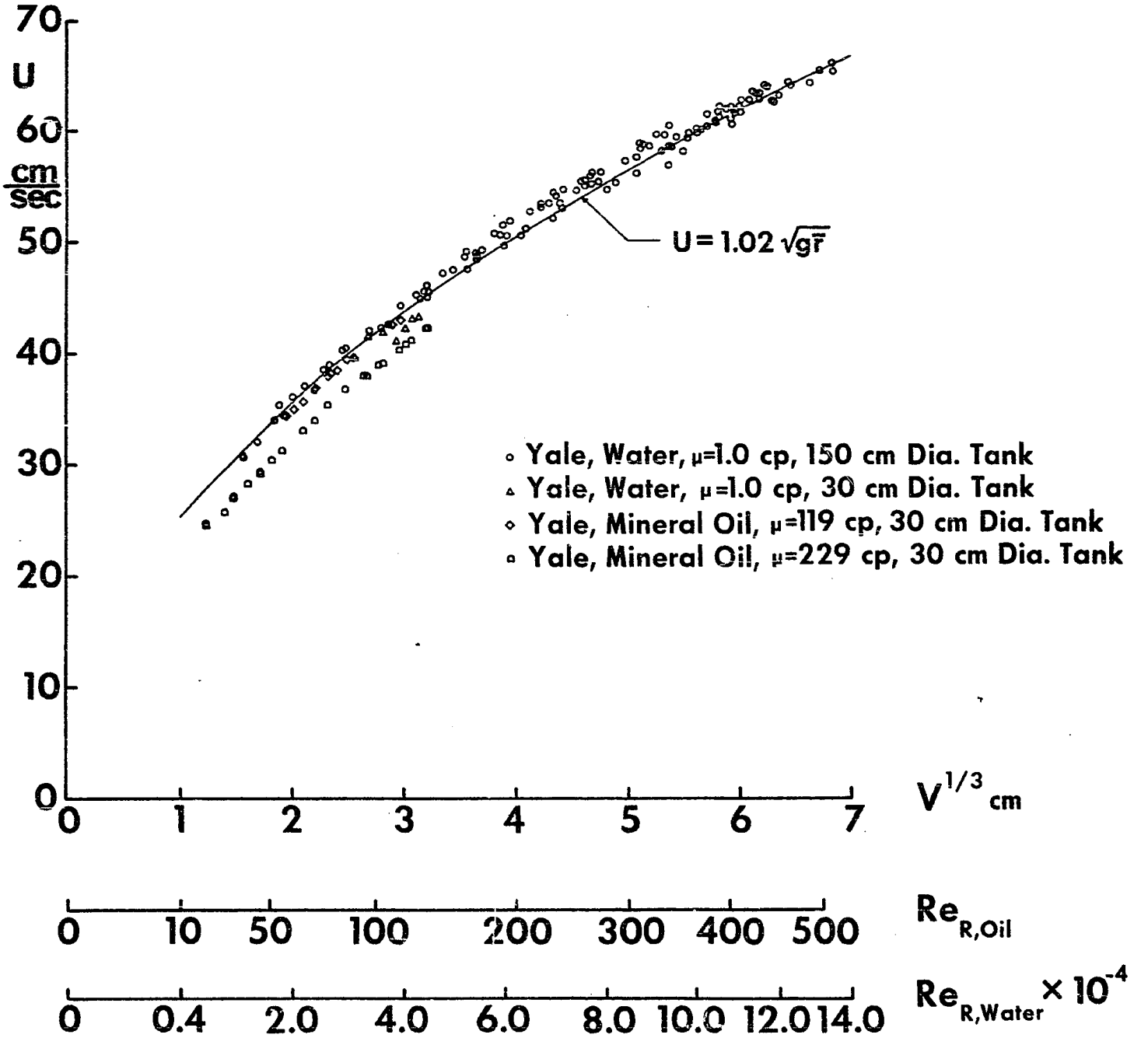

Reproduced with permission of the copyright owner. Further reproduction prohibited without permission.

Fig. 11

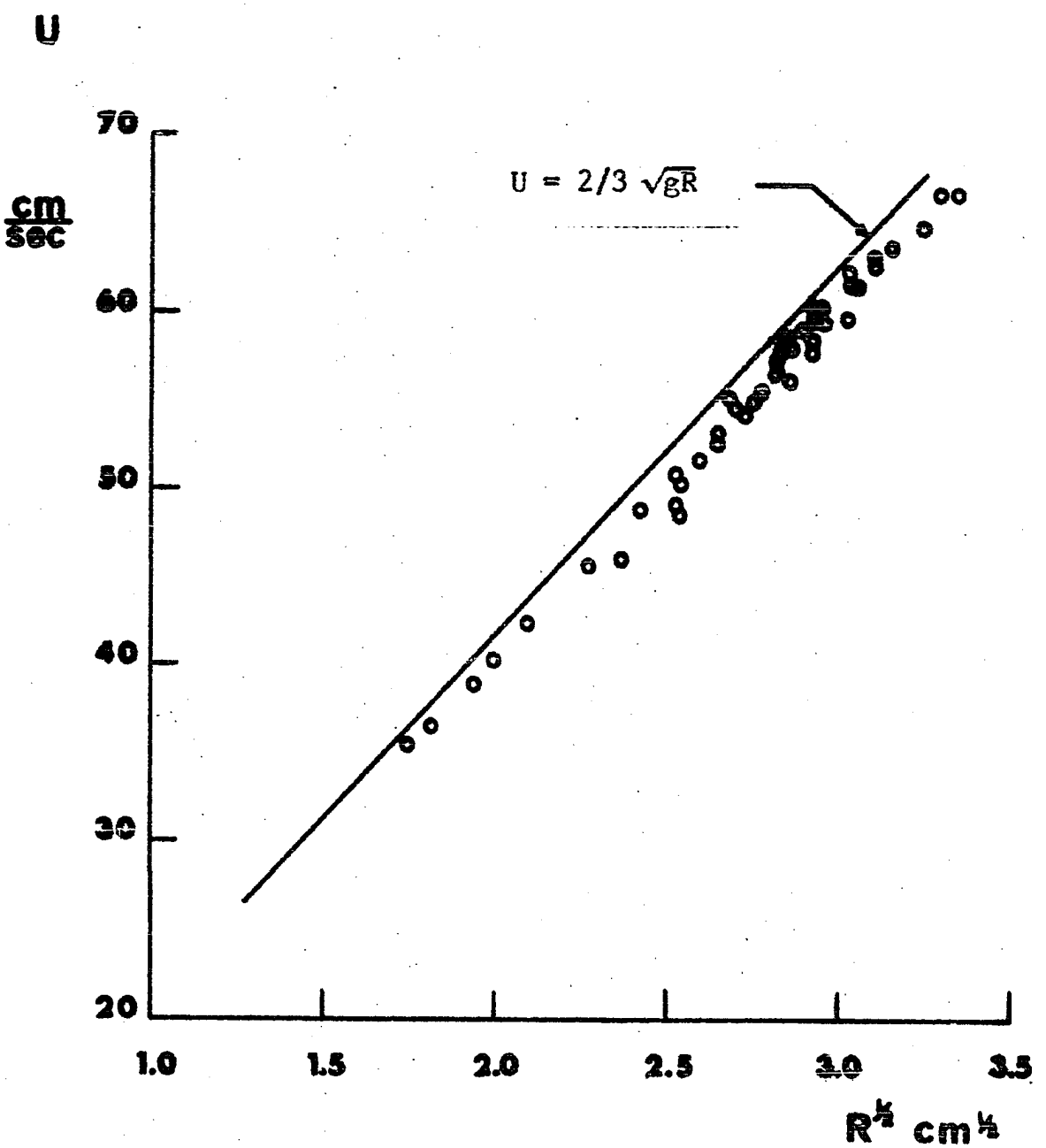

Reproduced with permission of the copyright owner. Further reproduction prohibited without permission.

Fig. 12

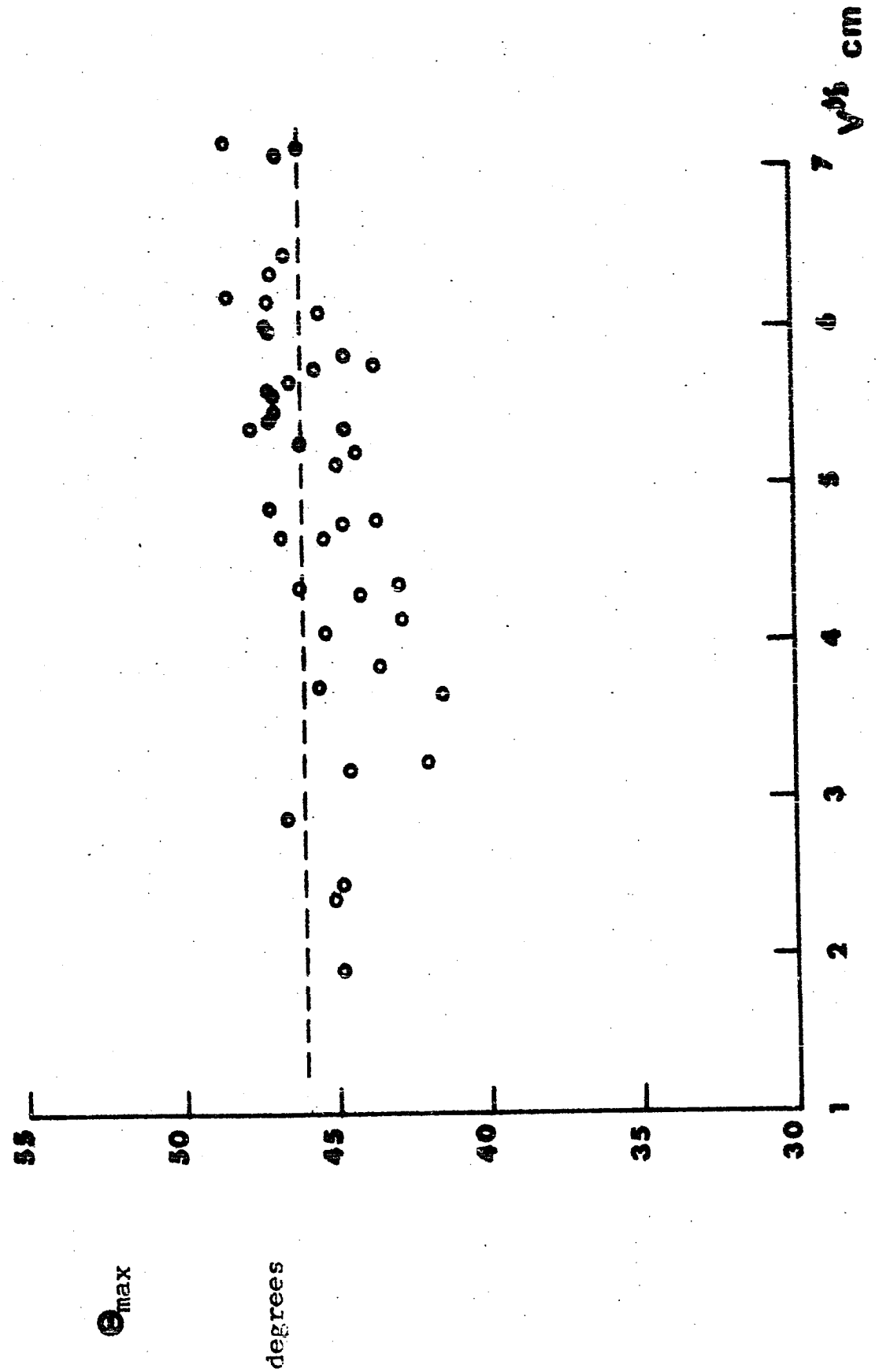

Reproduced with permission of the copyright owner. Further reproduction prohibited without permission.

Reproduced with permission of the copyright owner. Further reproduction prohibited without permission.

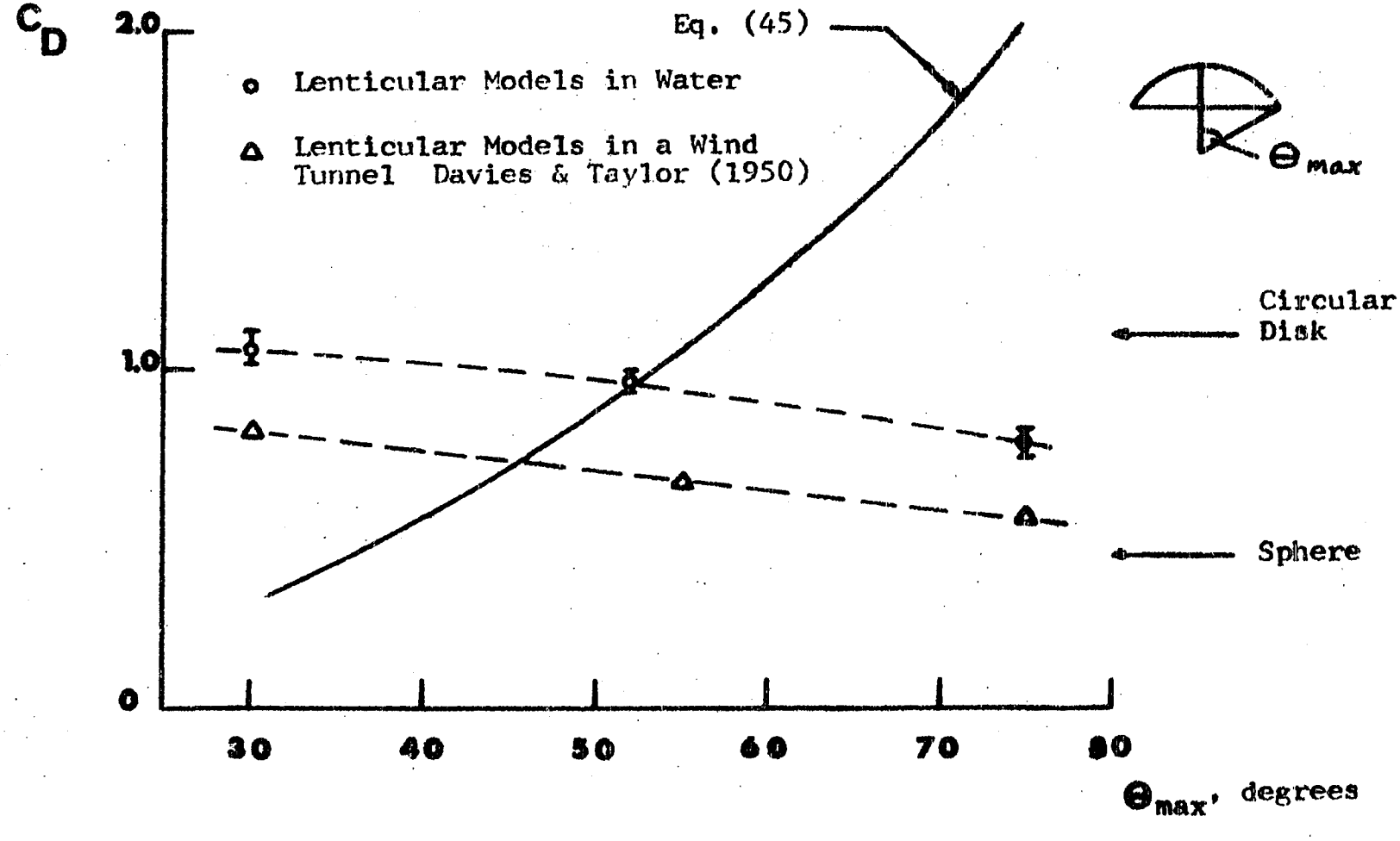

Fig. 13

Fig. 14

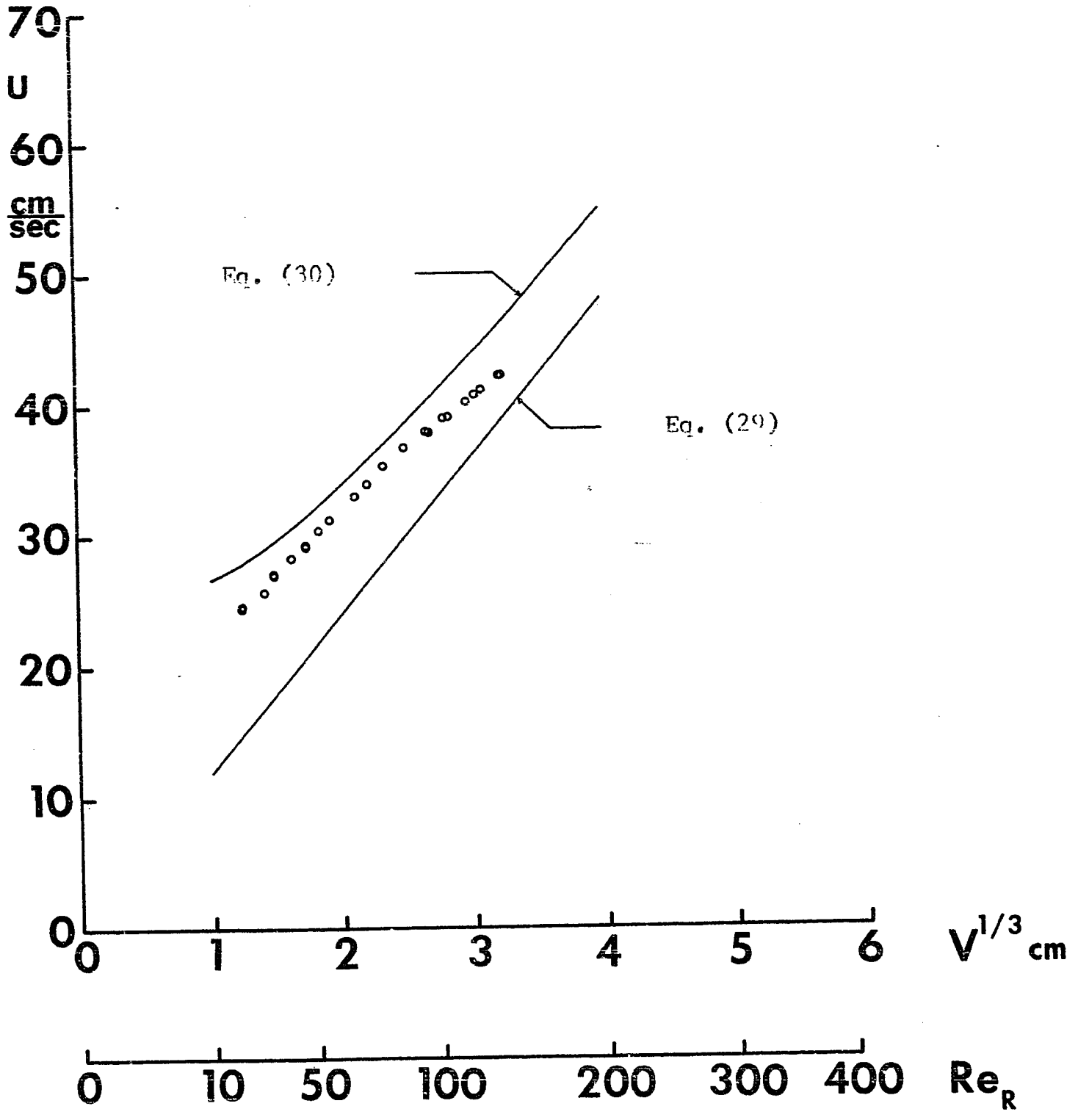

Reproduced with permission of the copyright owner. Further reproduction prohibited without permission.

Fig. 15

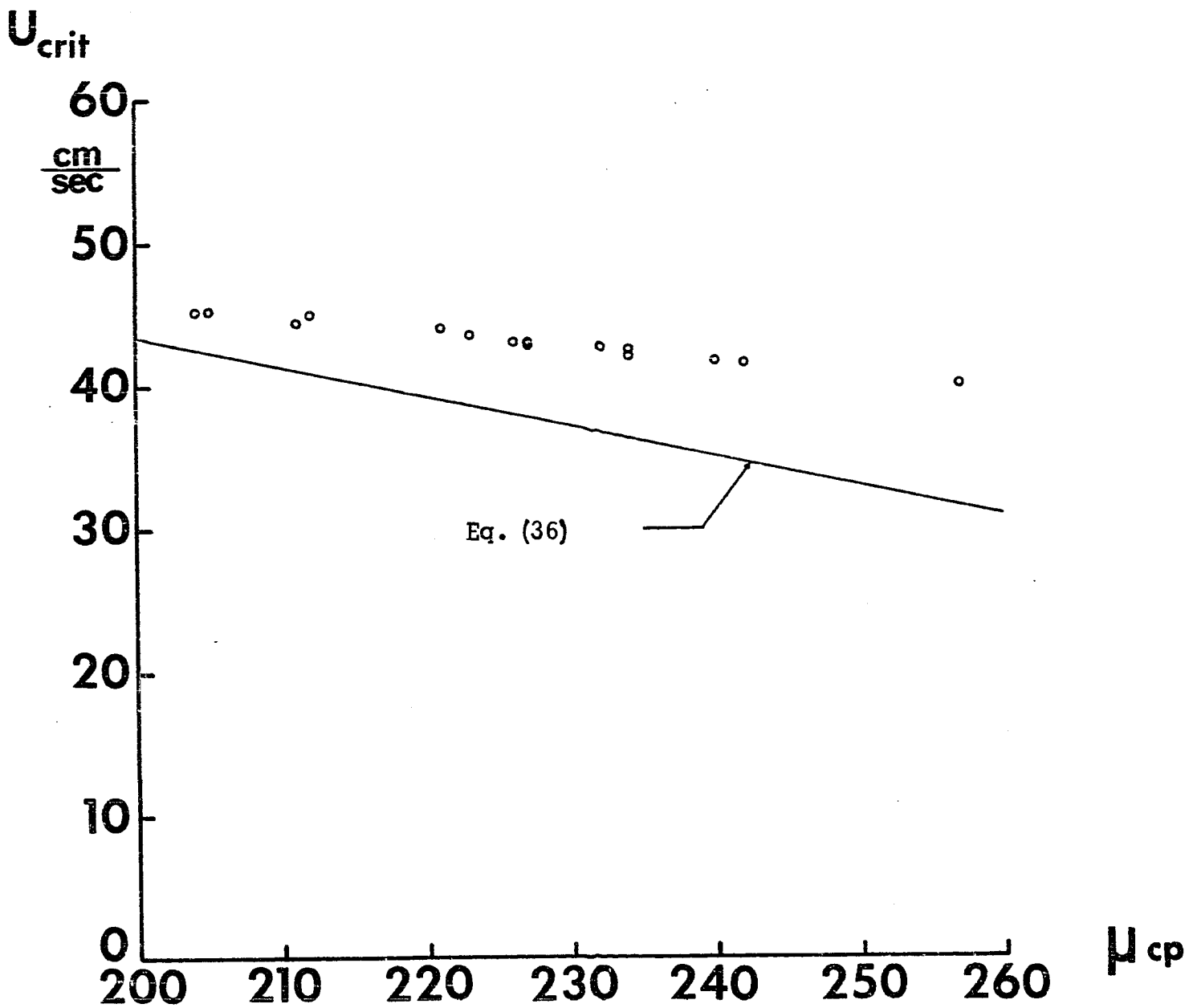

Reproduced with permission of the copyright owner. Further reproduction prohibited without permission.

Fig. 16

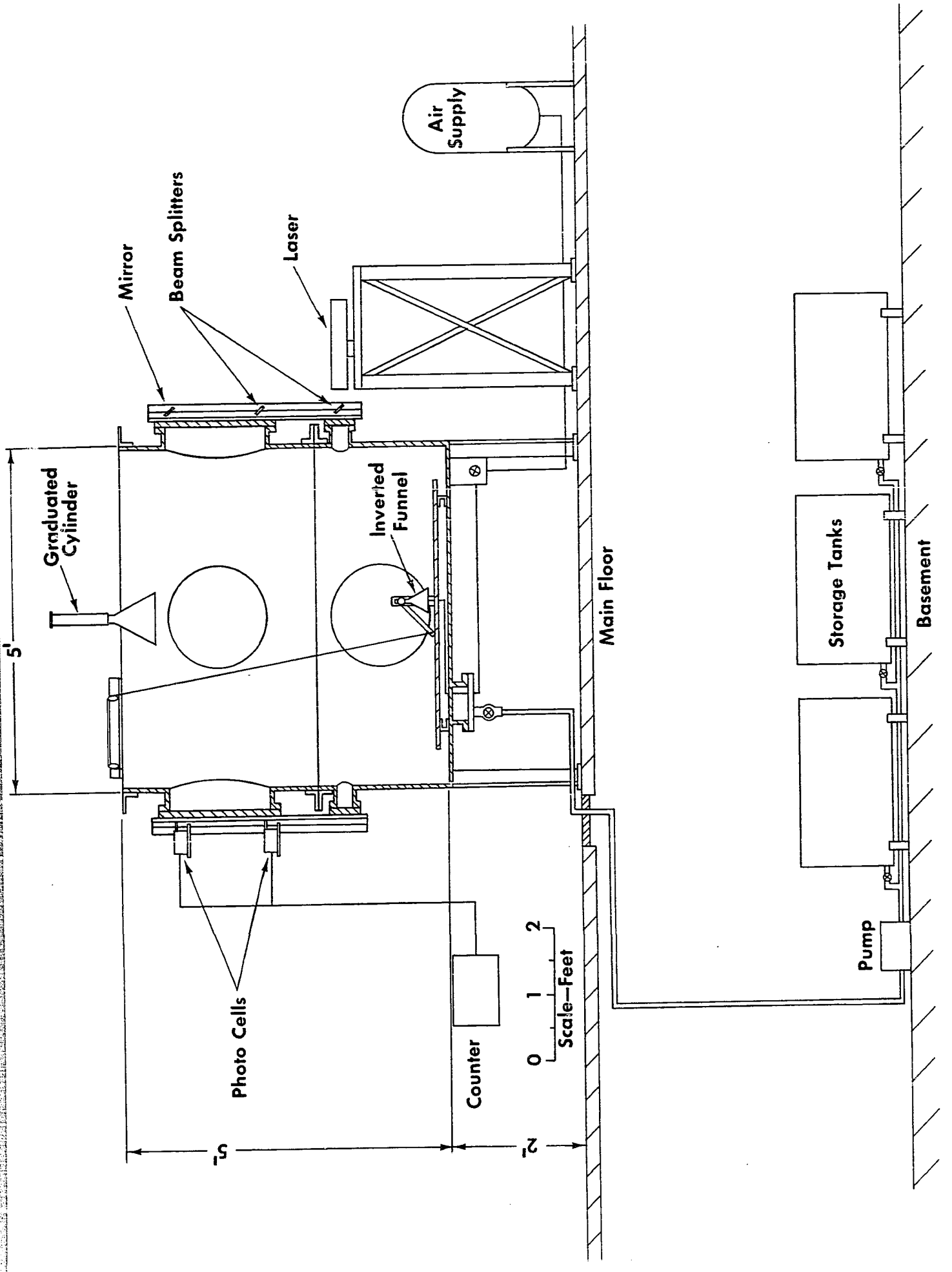

Reproduced with permission of the copyright owner. Further reproduction prohibited without permission.

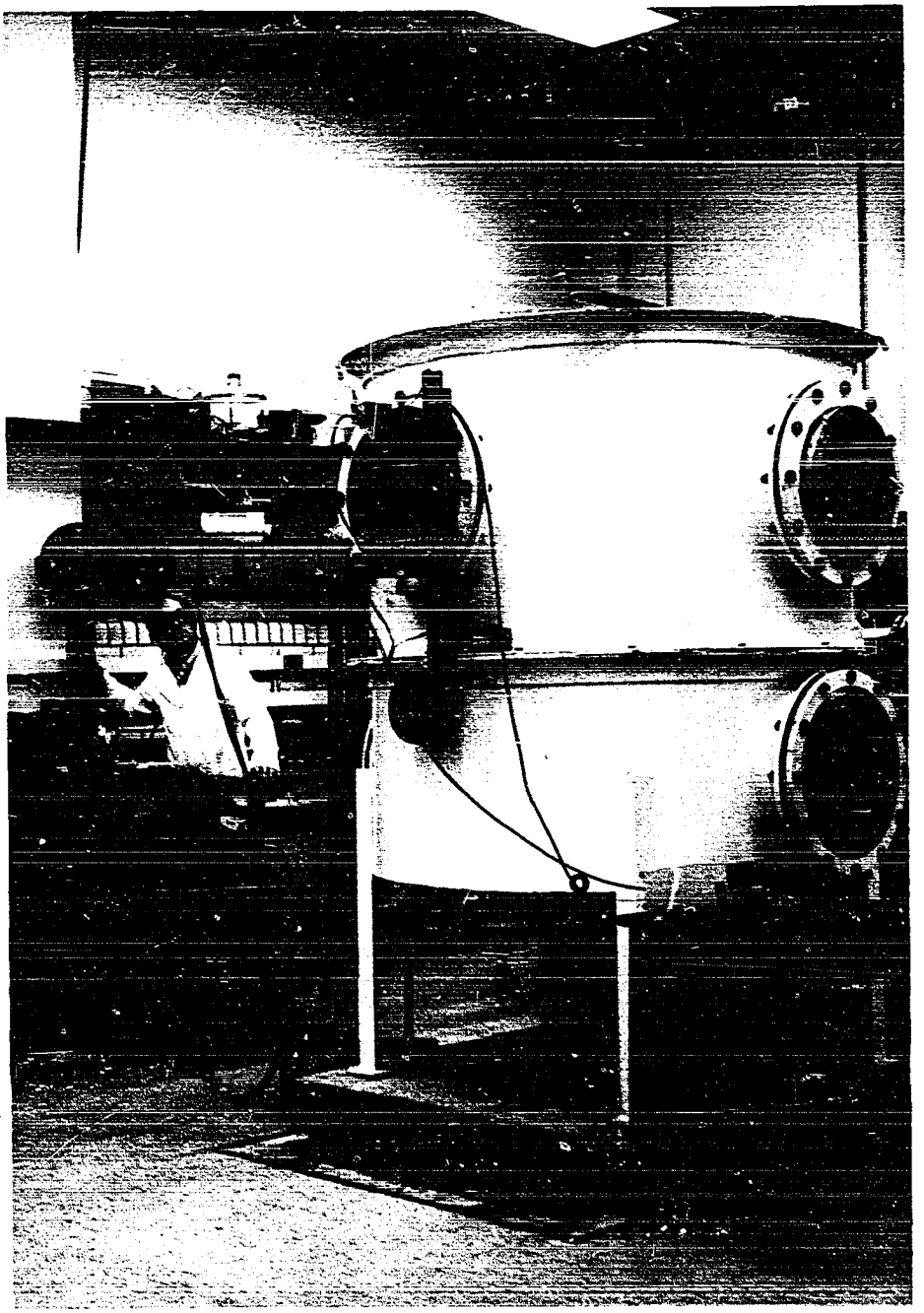

Reproduced with permission of the copyright owner. Further reproduction prohibited without permission.

Reproduced with permission of the copyright owner. Further reproduction prohibited without permission.

Fig. 19

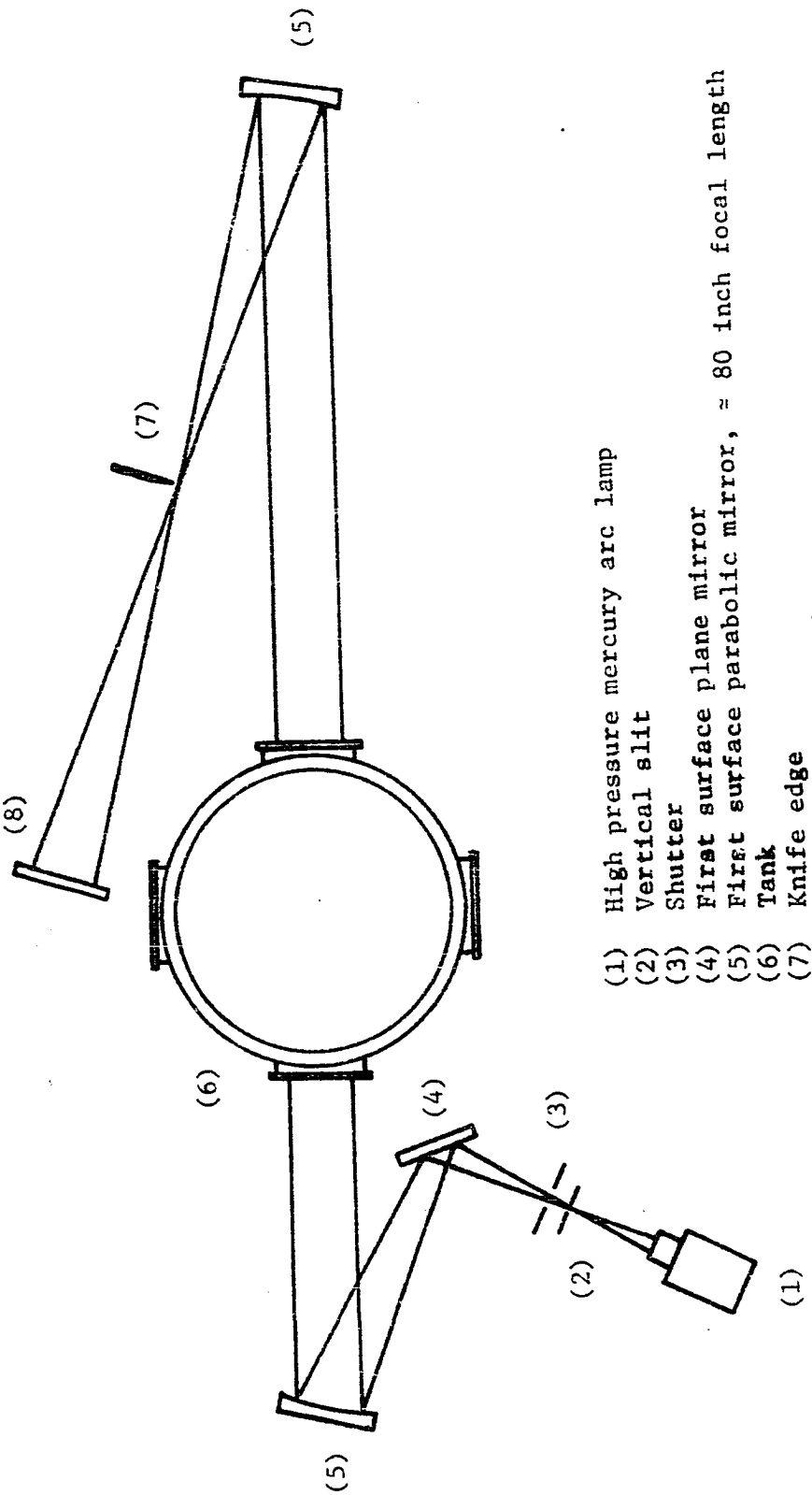

Reproduced with permission of the copyright owner. Further reproduction prohibited without permission.